Joan Renato Alain Barreda Concha

Bachelor of Science in Micro and Nanotechnologies Engineering

Mastering Jet Milling – developing process understanding through modeling and advanced characterization

Dissertation submitted in partial fulfillment
of the requirements for

Master of Science in
Micro and Nanotechnologies Engineering

Supervisor: Doutora Ana Raquel Xarouco de Barros, Scientist,
Hovione FarmaCiência S.A.

Co-supervisor: Prof. Doutora. Elvira Maria Correia Fortunato, Full professor,
Faculty of Science and Technologies, NOVA University of Lisbon

Júri

Chairperson: Prof. Doutor Rodrigo Martins

Raporteurs: Prof. Doutora Ana Pimentel

Member: Doutora Raquel Barros

FACULDADE DE CIÊNCIAS E TECNOLOGIA
UNIVERSIDADE NOVA DE LISBOA

October, 2019

Mastering Jet Milling – developing process understanding through modeling and advanced characterization

Agradecimentos

A realização desta tese significa para mim a fase que todos um dia devemos enfrentar; a de sair da nossa zona de conforto para tentar melhorar as nossas capacidades e amadurecer neste longo e único percurso. No final, o que importa é a experiência e a forma como sabemos lidar com todas as situações que se apresentam, e nunca poderia ter conseguido sem o apoio incondicional de todas as pessoas que me rodearam nestes anos todos.

Em primeiro lugar quero agradecer à Professora Doutora Elvira Fortunato e ao Professor Doutor Rodrigo Martins por terem criado o curso de Engenharia em Micro e Nanotecnologias, que foi a minha casa durante estes 5 anos, e que me permitiu poder ter uma formação universitária numa Faculdade tão conceituada como é a Faculdade de Ciências e Tecnologias da Universidade NOVA de Lisboa. Agradeço à Professora Elvira por permitir a realização da minha tese num espaço tão prestigiado como o CENIMAT, e ao Dr. Rafael Antunes, Diretor do Departamento de R&D Produtos, por me ter aceite no departamento de uma empresa tão prestigiada como é a Hovione FarmaCiência S.A.

Quero agradecer de forma muito sincera às minhas duas orientadoras; à Professora Doutora Elvira Fortunato e à Doutora Raquel Barros, por todo o apoio e paciência que tiveram comigo durante a minha dissertação; a vossa ajuda e compreensão foi essencial para que eu pudesse acabar a minha tese e mestrado. Muito obrigado.

A toda a equipa da Hovione FarmaCiência S.A., departamento R&D Produtos, ao Dr. Rafael Antunes, Director do departamento. A todos os cientistas, em especial à Margarida, à Luisa, à Andreia, ao Sérgio, à Sara Sequeira, ao Luis Sobral e ao Luis Gaspar, por me terem ensinado e apoiado com os equipamentos, e também por todo o que aprendi de vocês durante a minha tese. A todos analistas, em especial à Débora e à Sónia, por estarem sempre disponíveis e bem-dispostas para me ajudar e acompanharem dentro e fora do laboratório. À Ana Miranda, à Ana Paula Rodrigues e ao Sr. Zé, por me ajudarem tanto com os envios e as boleias, e por toda a paciência que tiveram quando só cometia erros nas marcações. Aos meus colegas e amigos que estagiaram comigo e que conheci no OnBoarding, Ivo, Inês, Sara, Rita, Bernardo e Francisco, pela vossa companhia que fez mais por mim do que possam imaginar. Aos técnicos de laboratório, Filipe, João Caetano, João Alcântara, Pedro Parreira e Pedro Dinis, e ao Salomão, vossa ajuda e companhia foi das mais essenciais de todas. Todos foram parte desta grande experiência que foi fazer a minha dissertação numa empresa com um ambiente de elevado profissionalismo e ao mesmo tempo descontraído o suficiente para dar as melhores condições de trabalho.

À equipa do CENIMAT e do DCM; à Sónia e à Daniela que me ajudaram imenso com as marcações dos equipamentos quando mais precisei. À Alexandra e à Sónia, por me terem orientado dentro do laboratório, e facilitado o meu trabalho fornecendo-me equipamentos e uma área de trabalho própria para mim e a minha colega Rita, muito obrigado. À Andreia e ao Professor Rui Silva do DCM, por me terem ajudado tanto com as resinas e o polimento das mesmas, assim como com as dúvidas que tinha sob a microindentação e a formação para usar o equipamento. À Daniela e ao Tomás, por todo o que fizeram por mim e por toda a compreensão, sem a vossa ajuda não teria conseguido acelerar o meu trabalho o suficiente para poder acabar as caraterizações a tempo, irei passar pelo DCM para vos agradecer pessoalmente um dia a vocês e ao resto de pessoas que de uma forma ou outra estiveram envolvidos no decorrer da minha tese.

Aos meus amigos e colegas da faculdade que foram um suporte fundamental para mim nestes seis meses, em especial ao João, à Inês e à Mafalda; vocês são de longe as melhores pessoas que conheci neste curso, estou ansioso por ver-nos crescer agora que acabamos o curso e ver até onde somos capazes de ir. Aos meus amigos de mais longa data, João, Diogo e Pedro; nunca irei poder retribuir o apoio que me deram nesta altura, não há forma em que vos possa expressar a gratidão que tenho por ter-vos conhecido, a melhor forma que tenho para o fazer é com um abraço.

Finalmente, à minha família. Si algún dia leen esto quiero que sepan que me mantuve de pie por ustedes, que las fotos de Ivane me hacian sonreir cuando más lo necesite, que se de algunas cosas que ya pasaron en la família y mismo asi estamos todos más unidos que nunca, que solo me hubiera gustado poder estar de una vez con ustedes en navidad cuando estaba escribiendo este texto; los quiero mucho. Y por último, a lo mejor que tengo y aún no se como; a mi mamá. Mamá, siempre estás

de mi lado sin importar lo que pase, aunque signifique que no duermas la noche entera para poder acompañarme, siempre estás ahí para darme ánimos, y eres el mejor ejemplo que he visto y he tenido, espero un dia ser tan buen padre y madre como tú lo eres para mi. No hay nada más que te pueda decir, apenas que un gesto dice más que mil palabras mamita. Te amo.

Resumo

Jet milling é um dos processos de redução de tamanho de partícula mais utilizados para obter partículas adequadas para a gama de inalação. A energia aplicada durante o processo de micronização depende de vários parâmetros de micronização, tais como pressão na câmara de micronização e caudal de alimentação, sendo que estes estão relacionados com as características físico-químicas do material de partida.

O principal objetivo deste trabalho foi identificar e relacionar as principais características do material de partida com os parâmetros de micronização de modo a construir um modelo que permita prever com base na caracterização do material de partida, quais os parâmetros de micronização para atingir um determinado tamanho de partícula reduzindo desta forma o número de testes do desenho de experiências.

Neste trabalho foram utilizados dois materiais de partida com diferentes características que foram em seguida micronizados utilizando diferentes condições de micronização (pressão e caudal). Tanto para os materiais de partida como para os materiais micronizados fez-se uma extensa caracterização das suas propriedades físicas, tais como tamanho de partícula, morfologia, cristalinidade, área superficial, densidade entre outras.

Um modelo PLS foi implementado, considerando as características dos materiais iniciais como variáveis X e as características dos materiais micronizados como variáveis Y. Várias análises estatísticas foram feitas até se obter um modelo final, no qual foi possível identificar as variáveis Y mais importantes e previsíveis pelo modelo, sendo estas Dv90, span, Dv50, SSA e APD. Com uma análise mais aprofundada do modelo final, foi também possível correlacionar estas variáveis direta e inversamente com cada variável X.

Palavras-chave: Jet milling, micronização, câmara de micronização, caudal de alimentação, modelo, PLS.

Abstract

Jet milling is one of the most widely used particle size reduction processes to obtain particles suitable for inhalation. The applied energy during the micronization process depends on several micronization parameters, such as the pressure inside the grinding chamber and the material feed rate, which are related to the physicochemical characteristics of the starting raw material.

The main objective of this work was to identify and relate the main characteristics of the starting raw materials with the micronization parameters in order to build a model that allows the prediction, based on the characterization of the starting raw material, of the required micronization parameters to achieve a specific particle size, reducing the number of experiment design tests.

In this work two starting raw materials with different characteristics were used and micronized using different micronization process conditions (grinding pressure and feed rate). An extensive characterization of physicochemical properties such as particle size, morphology, crystallinity, surface area, density, and other characteristics was performed for the starting raw and micronized materials.

A PLS model was implemented considering the starting raw and micronized material characteristics as X and Y variables, respectively. Several statistical analyses were also performed in order to obtain a final fitted model, in which the Dv90, span, Dv50, SSA and APD were identified as the most important and predictable Y variables. Further analysis of the fitted model allowed the observation of the correlation between the respective X and Y variables.

Keywords: Jet milling, micronization, grinding chamber, material feed rate, model, PLS.

Table of contents

List of figures

List of tables

List of Symbols

$\mathbf{A}$	Grinding nozzles total area
$\mathbf{Dv10}$	Particle size of 10% of the total volume of particles
$\mathbf{Dv50}$	Particle size of 50% of the total volume of particles
$\mathbf{Dv90}$	Particle size of 90% of the total volume of particles
$\mathbf{E_k}$	Gas kinetic energy
$\mathbf{k}$	Ratio of specific heats of the gas
$\mathbf{M_g}$	Gas mass flow rate
$\mathbf{M_w}$	Molecular weight of the fuel employed for grinding
$\mathbf{P}$	Absolute pressure of the gas used for grinding
$\mathbf{Q}$	Solids feed rate
$\mathbf{Q^2}$	Correlation coefficient of cross-validation
$\mathbf{R}$	Gas constant
$\mathbf{R^2}$	Correlation coefficient
$\mathbf{T}$	Gas temperature
$\mathbf{v_s}$	Gas sonic velocity

Acronyms

AFM	Atomic Force Microscope
APD	Average Pore Diameter
API	Active Pharmaceutical Ingredient
a.u.	Arbitrary units
BET	Brunauer-Emmett-Teller
CENIMAT	Centro de Investigação de Materiais
CI	Confidence Interval
CS	Crystallite Size
DPI	Dry Powder Inhaler
DMT	Derjaguin-Müller-Toporov
Esp	Micronization Specific Energy consumption
JM	Jet Milling
MVA	Multi-Variate Analysis
PCA	Principal component analysis
PLS	Partial Least Squares
pMDI	Pressurized Metered-Dose Inhaler
PSD	Particle Size Distribution
RMSEcv	Room Mean Square Error of cross-validation
SD	Standard Deviation
SEM	Scanning Electron Microscope
SRM	Starting Raw Material
SSA	Specific Surface Area
TPV	Total Pore Volume
VIP	Variable Importance for the Projection
XRD	X-Ray Diffraction

Confidentiality

Due to confidentiality reason, the APIs in study will be mentioned by their code name instead of their actual composition. Some bibliographic references will be omitted (every time it appears[1]) when it is considered that presenting these references could lead to the identification of the APIs studied.

Objectives

This work was realized at Hovione FarmaCiência S.A and at CENIMAT FCT-UNL. The main objective of this work focused on the implementation of a statistical model to enable the correlation and prediction of the characteristics of micronized materials obtained by jet milling technique.

For this purpose, two starting raw materials with different characteristics were milled using different micronization conditions. The characterization of the starting raw materials and of the micronized materials was performed by several techniques such as SEM, XRD, Laser diffraction, BET, and Helium picnometry. The micronized materials characteristics with the variation of the micronization main parameters, grinding pressure and the feed rate was studied.

The material used in this work was an API widely used for inhalation products in the pharmaceutical field. The acquired knowledge of this work will contribute to:

- Better understanding of the micronization process using a spiral JM process.
- Identify the most suitable process parameters to obtain materials in the inhalation range.
- Better understanding of the influence of the micronization process parameters on the micronized material characteristics.
- Better understanding of the impact of the starting raw material characteristics on the micronized material characteristics.

1 Introduction

1.1 Active Pharmaceutical Ingredients (APIs)

The pharmaceutical industry has always been one of the leading industries in the market, requiring greater quality control in products manufacturing. APIs are biologically active ingredients that are responsible for the pharmacological effect in the body; these combined with the excipients, which are the responsible for delivering the API to the affected location, are designated as pharmaceutical drug or medicine [1]. There are many types of pharmaceutical formulations that depend on the application and type of delivery.

Regarding pulmonary drug delivery, there are three main inhalation systems for the aerosolization of drugs: nebulizers, pressurized metered-dose inhalers (pMDIs) and dry powder inhalers (DPIs). Nebulizers are used to treat lung diseases, are often used for drugs that are only available in solution form and present two designs, pneumatic or jet nebulizers and ultrasonic nebulizers [2]. One of the main drawbacks of nebulizers is their efficiency as a large part of the drug is either retained in the nebulizer or exhaled. However, nebulizers also present less adverse effects due to the lower dose of the inhaled drug [3, 4]. DPIs are also widely used to treat pulmonary deceases and are known to be effective and efficient in drug delivery [5]. However, it is much more challenging the formulation process itself [3]. pMDIs are considered the most used inhalation system for the treatment of asthma [6]. pMDIs are only used for some drugs or dosages and also present inconsistent dosing mainly due to the incorrect use of the device [3].

It is important to have an efficient and reliable drug administration to the respiratory tracts in order to cause the desired therapeutic effect. Several properties were reported to be crucial as they affect the inhalation performance of dry powder inhalers.

1.2 Pulmonary Drug Delivery

For the treatment of respiratory diseases, inhalation therapies have been used over the years and have been gaining more importance in the research field [3, 7]. The efficacy of the treatment depends on several factors such as the effectiveness of the technique, which is related to the control of the drug delivery in the affected area. A controlled drug delivery presents several advantages, it improves the bioavailability by controlling the drug release, and reduce harmful and side effects by acting only in the affected area [8].

The PSD was reported to be one of the most important properties of drugs for inhalation as only particle sizes lower than 5 µm can reach the lower respiratory tracts, having a crucial impact on the formulation performance affecting their solubility, flowability, stability, and other properties [9–12]. Depending on the size-reduction process, the decrease of particle size may lead to an increase or decrease of the surface area of the particles [13], which may affect their performance as mentioned in a previous work, where an increase of SSA led to an increase of the solubility of the drug API, improving its bioavailability [14]. Although smaller particle sizes are required for inhalation, larger surface areas may lead to greater moisture uptake, which would eventually affect the aerosol generation and lung deposition [15, 16]. The moisture uptake was reported to influence DPIs by the respirable fraction, that is, their efficiency [17]; and pMDIs, compromising its physical stability and drug delivery performance [6].

The morphology of the APIs is known to affect the performance of pharmaceutical powder aerosols by affecting their aerodynamic properties [18].

The determination of the polymorphic form of the materials used for dry powder inhalers is crucial for the formulation, as different polymorphs present different properties such as density and hardness, that may affect their performance; e.g., dissolution rate and solubility [19]. Other properties, such as density and cohesive forces were also mentioned to be relevant [19]. Therefore, it is essential to control the drug product manufacturability and assess their performance for each application.

The particle size of bulk APIs is generally larger than the required specifications and must be decreased by employing grinding and milling techniques in order to reach a particle size lower than 5 µm, as mentioned before. Decreasing the particle size by milling may enhance their performance; e.g., increase the solubility of the milled particles by increasing the density of the obtained materials, but also

induce undesired properties, as the properties of the materials may change after the micronization process and even upon storage [20–22].

1.3 Micronization process

There are various types of micronization processes: spiral or loop jet mills, impact and counter flow jet mills, that use fluid energy for the grinding process and are selected following the specifications and desired final particle properties [23]. The main parameters of each milling equipment vary, e.g., spiral jet mills use as main parameters the grinding pressure inside the micronization chamber and the solids feed rate, while impact mills such as the pin mill use the speed of rotation and the solids feed rate [24]. Although there are various types of milling processes, only a few are suitable to obtain the required particle size for inhalation [16], such as fluid-energy mills (jet mill), high-peripheral-speed mills (pin mill), and the ball mill. The jet mills are the most suitable equipment for inhalation since it is possible to obtain particle sizes lower than 1 µm and also present several advantages such as narrower PSD, ease of cleaning that allows to perform several tests, and simplicity [25]. Pin mills use mechanical impact in order to decrease the particle size; compared with the jet mill, it uses less energy consumption but is not possible to reach a small particle size as for the last-mentioned [16]. However, being a high energy process, milling may have a severe impact on the micronized material characteristics, e.g. undergoing micronization may change their crystal structure, polymorphic form, and morphology, and consequently affect their bioavailability, stability and other crucial properties [13].

1.4 Description and operating principle of a classic spiral jet miller

An example of a spiral jet mill is presented in Figure 1.1. The feed material is introduced into a product funnel and is driven using an injector gas which can be air, nitrogen or vapor inside the micronization chamber. The gas expands through grinding nozzles that are located in tangential positions inside the grinding chamber [26]. Two types of grinding nozzles can be used; converging nozzles and Laval type nozzles, being the first-mentioned the most common type. Each type of nozzle leads the gas into sonic and supersonic velocities inside the grinding chamber, creating a vortex [25]. This vortex induces particle-particle and particle-wall collisions that lead to a decrease in the material particle size. The particles inside the grinding chamber are subjected to centrifugal and drag forces. These forces are opposite and depend on the material (e.g. mass, speed of the particle), on the milling conditions (e.g. speed and vector of the flowing gas) and the grinding chamber (chamber geometry) [27]. The main micronization process parameters are the grinding pressure in the micronization chamber and the material feed rate [25]; both parameters greatly affect the final particle size that is obtained in the micronization process. The grinding gas pressure and the material feed rate can be adjusted in order to increase or decrease the intensity of particle-particle collisions and the residence time, respectively [28], which determine the particle size of the obtained micronized material.

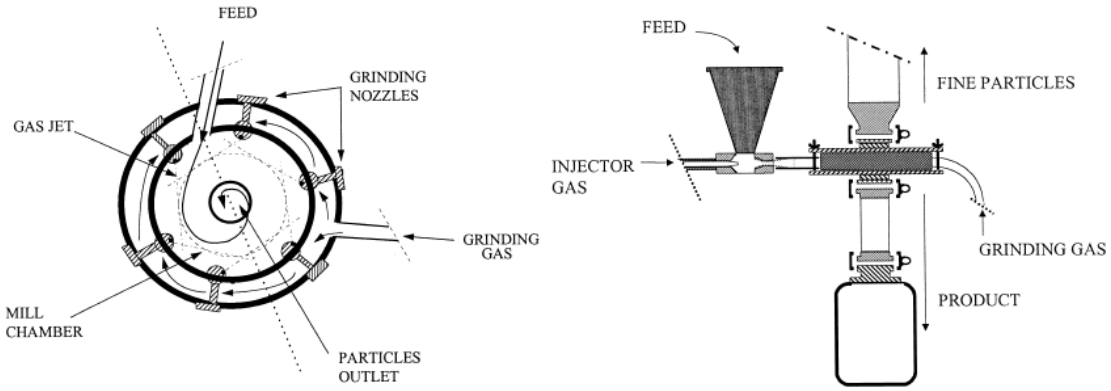

Figure 1.1: Scheme of a spiral jet mill [23].

The grinding ratio of a spiral jet mill is greatly affected by the mill design and the grinding process parameters. Regarding the mill design, parameters like the size of the milling chamber, its shape and the number and angle of the grinding nozzles are crucial [23]. Several studies were performed in order

to study the effect of micronization process parameters in the micronized material physical-chemical properties.

The grinding power supplied as a gas kinetic Energy (E_k) for sonic nozzles can be expressed [29] by:

$$E_k = \frac{1}{2} M_g {v_s}^2 \tag{1.1}$$

where v_s is the gas sonic velocity and M_g is the gas mass flow rate that is expressed [23] by:

$$M_g = PA\sqrt{\frac{M_W k}{RT}\left(\frac{2}{k+1}\right)^{\frac{k+1}{k-1}}} \tag{1.2}$$

where:

P is the absolute pressure of the gas used for grinding,

A is the grinding nozzles total area,

M_W is the molecular weight of the fuel employed for grinding,

k is the ratio of specific heats of the gas,

R is the gas constant,

And T is the gas temperature.

In order to include, in the same parameter, both grinding pressure and solids feed rate, the notion of Micronization Specific Energy Consumption (Esp) is used [29] :

$$E_{sp} = \frac{E_k}{Q} \tag{1.3}$$

where Q is the solids feed rate.

The specific surface area (SSA) of the product is related to Esp by a power function:

$$SSA \propto E_{sp}^{x} \tag{1.4}$$

The representation of the product SSA vs Esp provides a physical understanding of the influence of grinding pressure and solid feed rate on the grinding ratio.

$$E_{sp} = \frac{E_k}{Q} \propto \frac{P}{Q} \tag{1.5}$$

Since the ratio between grinding pressure and feed rate is proportional to the Esp; thus, higher grinding pressure and lower feed rates increase the Esp used in the process.

Micronization using a jet mill equipment, as already mentioned, improves the bioavailability of the materials by obtaining a narrow PSD, enables the micronization of heat sensitive materials due to a low temperature process, and facilitates the cleaning and inspection of the mill parts. The main drawback of the Jet mill is the high amount of energy of the process [26], which conditions the number of tests that are performed and also affect the properties of the micronized materials, as mentioned before**.**

1.5 Influence of the milling process on the material characteristics

As mentioned before, the PSD reduction is crucial for the development of drugs in the pharmaceutical industry. Being a high energy process, milling may induce a change on the material properties, e.g. induce amorphization [30] and change its morphology [31]; thus, the physicochemical characterization of the initial and micronized materials is crucial since milling may compromise biopharmaceutical

properties such as the solubility and permeability of the APIs [32]. It was stated that material properties such as size, shape, bulk density, and others have an impact on particle size reduction [33].

Several properties such as morphology, crystal structure, mechanical properties like hardness and Young modulus, density, and surface area were reported to have an impact on the milling process [18, 31, 34, 35]. Consequently, these same properties could be largely affected during the micronization process [21, 36, 37].

Chikhalia et al. [31] studied the influence of two jet mill types on the properties of β-succinic acid crystals with plate and needle-like morphologies, proving that both mill types and the initial morphology affected the degree of crystallinity of the micronized crystals. It was also observed that the micronized material morphology was the same for both materials despite having different initial morphology.

The crystallinity of the material is also a very important property [38]; techniques like DSC and XRD are widely used in the pharmaceutical industry for the identification of polymorphs and the degree of crystallinity of the material [39]. Milling can induce the formation of amorphous regions on the micronized particles; over time the micronized particles tend to recrystallize which leads to changes in critical particle properties such as particle size distribution and morphology [36]. However, the stability of the final micronized material is crucial since a physical transformation could affect its bioavailability [40]. To overcome this issue, post conditioning treatments can be performed [41].

Mechanical properties such as hardness and Young modulus are also crucial parameters that influence the micronization process; where hardness correspond to the resistance of material to undergo plastic deformation and Young modulus correspond to the resistance of material to undergo elastic deformation. Micronization requires a full particle breakage of the material, that is, the energy used in the process must be sufficient to overcome the elastic properties of the material, as mentioned by Saleem et al. [34], who also studied the mechanical properties of a soft material, and concluded that between hardness and young modulus, the second affected more the necessary Esp for size reduction. The results obtained by Zügner et al. (2006) showed that different material properties such as hardness, young modulus, and density affect the breakage behavior of the materials during the milling process. As an example, harder materials require a higher Esp to break than softer materials. Other properties such as hygroscopicity, melting point and thermolability also affect particle size reduction, as stated in a more recent work [42]. PSD reduction could lead to an increase in surface area, which also increases the solubility of the APIs [43]. A study of the JM process was made by Nakach et al. [21], in which they stated the existence of two regimes of particle size reduction process; fragmentation at lower Esp and attrition at higher Esp. The variation of the surface area depends then on the domain on which the material is micronized; in the fragmentation regime an increase of surface are is verified with the increase of Esp; however, unlike particles micronized at lower Esp, the surface area of particles micronized at higher Esp change after micronization, due to a surface rearrangement upon storage, which may compromise other crucial properties.

1.6 Statistical model - MVA

A statistical model is a mathematical based model and powerful technique that allows prediction of new data by analysing previously obtained data, that is, it describes the relation between the dependent and the independent variables) [44].To implement a statistical model it is important to select the appropriate functional form and the respective probabilistic assumptions that better fits the data. Considering only the most significative variables for a model in order to improve its predictive ability is also important. Statistical models are used on several fields, such as environmental science, bioinformatics, natural language processing, and others; with different emphasis for casual explanation and empirical prediction depending on the field in which they are implemented [45].

A Multi-Variate Analysis (MVA) is the analysis of different variables of a process that involve several correlated observations. There are various methods to perform multivariate analysis, in which are included the Principal Component Analysis (PCA), the Partial Least Squares (PLS) and others [46]. PCA is a dimension reduction technique widely used to solve multi-collinearity problems and to reduce the number of independent variables to a suitable number that most contributes for a dependent variable. However, for cases with several dependent and independent variables and it is important to study their relation, PLS method is the most suitable method [46].

The PLS is a widely used projection method. It summarizes the X-variables, also referred to as the independent variables; and the Y-variables, which are dependent on the X-variables. As there are many X and Y-variables, the observations are distributed in space; a line that explains the largest possible

variance is traced between the points, this is called the first principal component. The second principal component explains the next highest variance and is obtained by the same method. As the first and second component are perpendicular, a plane is formed and the observations projected inside it forming the scores plot, as represented in Figure 1.2.

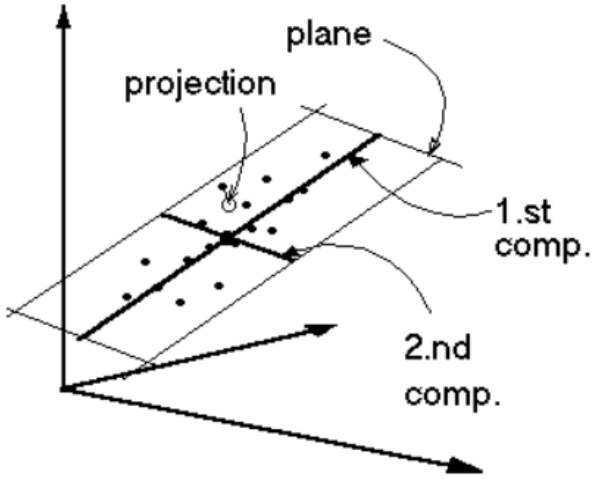

Figure 1.2: Principal components obtained from the observations plane [36].

A model is evaluated by the goodness of fit (R^2) and its predictive ability (Q^2), both values concerning only the Y-variables of the model. It must be stated that the R^2 will always increase with the increasing number of observations in the data. However, the Q^2 has a maximum value, that may decrease if more observations are added. Thus, there must be a trade-off between these variables [48].

The value of these variables is highly dependent on the field they are applied [49]. However, models with values of R^2 near 1 and Q^2 higher than 0.5 are considered good models Nevertheless, the difference between these values should not be more than 0.2 – 0.3 [50, 51].

2 Materials and Methods

2.1 Starting raw material

In order to perform the study using the micronization technique of JM, it was decided to use an API for formulation in inhalation, IH04, due to the impact that the physical properties could have on this type of formulation. Two starting raw materials (SRMs) of IH04 with different particle size were used, 05IH04.HM00003 and 06IH04.JCN003 as presented in Table 2.1. The SRM 05IH04.HM00003 was produced at Hovione site in Macao and from this material the SRM 06IH04.JCN003 with a smaller particle size was obtained via a manual grinder, a mortar.

Table 2.1: Dv10, Dv50 and Dv90 average values (n=3) and span for the SRMs

Starting raw material	Dv10 (µm)	Dv50 (µm)	Dv90 (µm)	Span
05IH04.HM00003	2.08 ± 0.17	8.93 ± 0.10	19.20 ± 0.07	1.78
06IH04.JCN003	1.53 ± 0.02	5.86 ± 0.05	14.07 ± 0.11	2.14

were Dv10, Dv50, and Dv90 correspond to the point in size distribution were 10%, 50% and 90% of the total volume of particles are contained.

2.2 Micronized material

The micronization equipment used was the LaboMill (F.P.S. Food and Pharma Systems), available at Hovione FarmaCiência S.A., designed to work with air and/or nitrogen as process gas. The feeding system consisted on a vibratory feeder; whose vibration is controlled trough a nitrogen flow. This equipment is presented in Figure 2.1.

A set of experiments was designed by varying the main process parameters of the JM process, the grinding pressure and the feed rate in order to observe the impact of each variable individually and of the specific energy. These conditions are summarized in Table 2.2. The injection line pressure was always 1 bar above the grinding line pressure to ensure the total entry of the product into the micronization chamber.

Table 2.2: Micronization conditions for the SRMs 05IH04.HM00003 and 06IH04.JCN003.

Starting raw material	Esp (kJ/kg)	Feed rate (g/h)	Grinding pressure (bar)	Micronized material (06IH04M.)
05IH04.HM00003	180.31	72.24	2.0	JCN006
	252.06	86.13	4.0	JCN007
	290.01	112.29	6.5	JCN008
	443.76	63.60	5.5	JCN020
	634.98	34.19	4.0	JCN015
	689.20	40.95	5.5	JCN016
	944.23	29.89	5.5	JCN017
	1148.07	18.91	4.0	JCN014
	1231.37	22.92	5.5	JCN005
	1232.82	17.61	4.0	JCN010
	2207.79	5.90	2.0	JCN009
	2252.07	14.46	6.5	JCN013
	3043.45	4.28	2.0	JCN018
	3111.68	9.07	5.5	JCN019
	4632.27	7.03	6.5	JCN012
	7003.20	4.65	6.5	JCN011
06IH04.JCN003	292.32	44.56	2.0	JCN025
	975.29	22.26	4.0	JCN026
	2156.07	13.09	5.5	JCN027
	6798.51	4.79	6.5	JCN028

Since the feeding system was controlled by a flow of nitrogen, in order to obtain the desired feed rate of each experiment, several tests were performed prior to each micronization. These tests simply consisted on feeding material during a certain amount of time and afterwards weight the obtained material. The feed rate was calculated by:

$$Q = \frac{\text{Obtained material (grams)}}{\text{time (hours)}} \tag{2.1}$$

The nitrogen flow was adjusted until the desired feed rate was achieved. If necessary, adjustments to the flow of nitrogen were performed. For the initial micronization tests, control of the particle size was performed in the middle of each process, in order to evaluate if the particle size was the expected one or if a feed rate adjustment was necessary. Once the process finished, the micronized material collected from the chamber and the filter were stored at low temperatures in order to study the obtained micronized materials and avoid structural changes such as recrystallization. Aproximately 3 g of each micronized material was obtained and were necessary to perform their characterization.

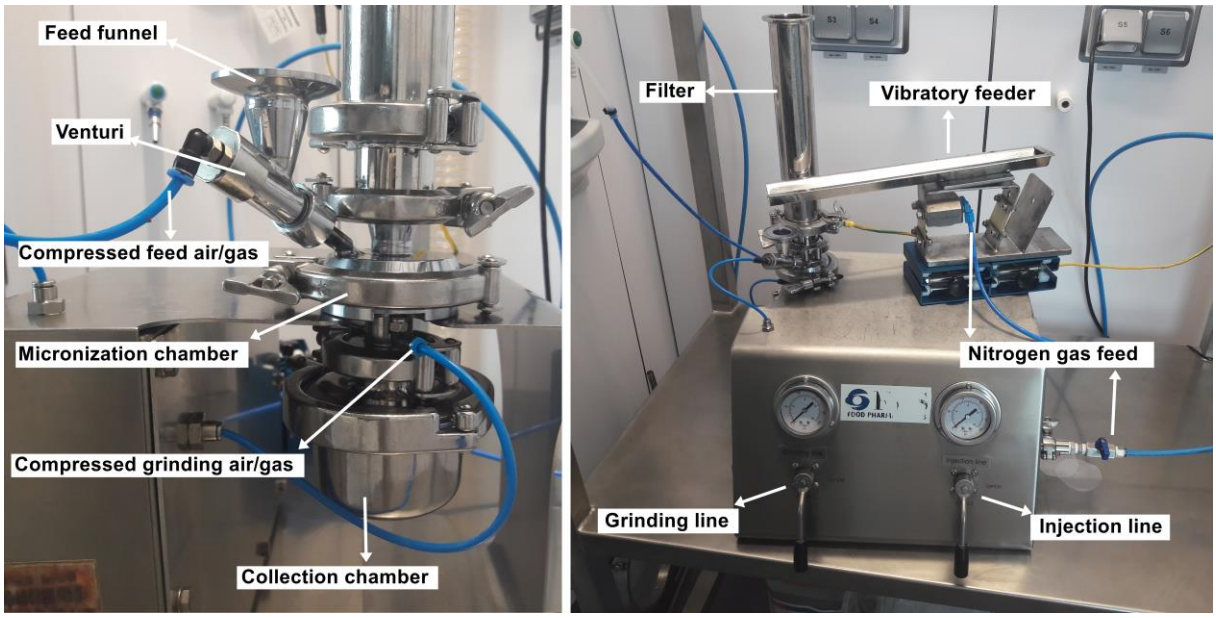

Figure 2.1: LaboMill and vibratory feeder equipment used for micronizations.

2.3 Material characterization

Except for the mechanical properties measured by nanoindentation for the SRMs, the same characterization techniques presented below were used to characterize both SRMs and micronized materials.

Morphology

The morphology of the particles was characterized by SEM using a Zeiss Auriga SEM-FIB Crossbeam workstation instrument, available at CENIMAT. Images were obtained using an acceleration voltage of 5 kV, and at ampliations of 2kX for the SRMs and 5kX for the micronized materials.

Crystallinity, polymorphic form, and crystallite size

The crystallinity, polymorphic form, and crystallite size (CS) were obtained by X-ray diffraction technique using an X-ray diffractometer (PANalytical's X'Pert PRO MRD) available at CENIMAT. The diffraction patterns were obtained using the Bragg-Brentano diffraction geometry, with a copper anode (Cu-Kα) as the X-ray radiation source (λ = 1.540598 Å). The scans were made ranging from 5° to 40° 2θ with a step size of 0.0167° and a time per step of 1 s. The diffractograms obtained were analysed using the HighScore Plus software. The CS was also obtained using this software, considering the Scherrer method and only the peak at approximately 24.35° 2θ.

Nanoindentation by AFM

Mechanical properties, hardness and Young modulus were measured by nanoindentation technique using an AFM-Asylum MFP3D available at CENIMAT. In order to avoid the movement of the particles during the nanoindentation process, the material was immobilized on an epoxy resin. Before the nanoindentation, a surface scan was performed using the tapping mode on the particles in order to define the number of points and the locations in which the nanoindentation would be performed. For each batch, several indentations were made on each particle for a total of 12 particles in order to obtain more accurate results.

The mechanical properties were measured by force spectroscopy with deflection as the trigger channel. A cantilever with a pyramidal tip and known mechanical properties was put in contact with the material surface at constant indentation force of 600 nN, which generated a surface area as a function of the indentation depth.

Several particles were indented, and an in-situ imaging of the indented surfaces was performed using the AFM software, obtaining the approach-retrace plots. These plots were used to measure the

interaction forces between the cantilever tip and the surfaces, and the data was used to quantify the mechanical properties of the materials, using the DMT model, suggested by the AFM software.

Particle size distribution

The particle size distribution was measured by the laser diffraction method. This light scattering method is based on the Fraunhofer mathematical model theory used to evaluate the PSD of a material, covering a wide range from submicron to millimeter scale. A laser beam passes through the material, being scattered at a wide range of angles and collected by detectors that measure their intensity.

The PSD parameters (Dv10, Dv50, and Dv90) were measured by this technique using a Sympatec, equipped with different modules attached to a HELOS diffractometer (configuration of HELOS/RODOS + ASPIROS) available at Hovione FarmaCiência S.A. The samples were filled in glass vials and inserted into the ASPIROS module, being subsequently released into the RODOS injector and passing through a laser for the PSD measurements. Three trials were made for each sample using the appropriate lens, R2 for a range from 0.45 µm to 87.5 µm and R1 for a range from 0.18 µm to 35 µm for the starting raw and micronized materials, respectively. For the starting raw materials, the dispersing method had a pressure of 0.3 bar and a feed velocity of 18 mm/s, while for all the micronized material samples the dispersing method had a pressure of 4 bar and a feed velocity of 50 mm/s. The span for each batch was also calculated using the obtained PSD values using the formula:

$$\text{span} = \frac{\text{Dv}_{90} - \text{Dv}_{10}}{\text{Dv}_{50}} \tag{2.2}$$

Specific Surface Area, Porosity and Density

The specific surface area (SSA) and porosity measurements were performed on a Micromeritics ASAP 2000 instrument using the BET adsorption method. This method used nitrogen (99.8%) as process gas with an effective section of 162 nm². Samples were evaluated by Multipoint at liquid nitrogen temperature and in a range of 0.05 to 0.35 relative pressures. Regarding porosity, the Average Pore Diameter (APD) and the Total Pore Volume (TPV) values for each sample were also obtained. The errors of equipment for these measurements were 2.40 m²/g, 0.10 nm, and 0.004 cm³/g for the SSA, APD, and TPV, respectively.

The real density of the raw and micronized particles was measured by Helium picnometry, using a Micromeritics AccuPyc 1330 model. Both equipment are available at IPN, Coimbra, Portugal.

2.4 Statistical model

The statistical model was implemented using the SIMCA software and a derived partial least squares (PLS) regression was used to model the data.

To obtain the final fitted model, different statistical analyses were performed, considering at an initial stage the characteristics of the starting raw and micronized materials summarized in Table 2.3, as well as the micronization process parameters. The X-variables, Y-variables, and the observations were therefore analysed in order to obtain a final fitted model for its interpretation and following prediction.

Table 2.3: Starting raw and micronized material characteristics considered as X and Y-variables, respectively, for the model implementation.

X-variables **Characteristics of the starting raw material**	**Y-variables** **Characteristics of the micronized material**
Dv10	Dv10
Dv50	Dv50
Dv90	Dv90
Span	Span
SSA	SSA
APD	APD
TPV	TPV
Density	Density
CS	CS

3 Results and Discussion

3.1 Characterization of the starting raw material

PSD

The PSD curves for the SRMs 05IH04.HM00003 and 06IH04.JCN003 are presented in Figure 3.1. The manual grinding led to a decrease of the PSD as observed in Table 2.1, as expected. However, the span (equation (2.2)) that correlate the 3 distribution variables increased with the decrease on the PSD. This could be related with a non-uniform manual grind of the SRM 06IH04.JCN003.

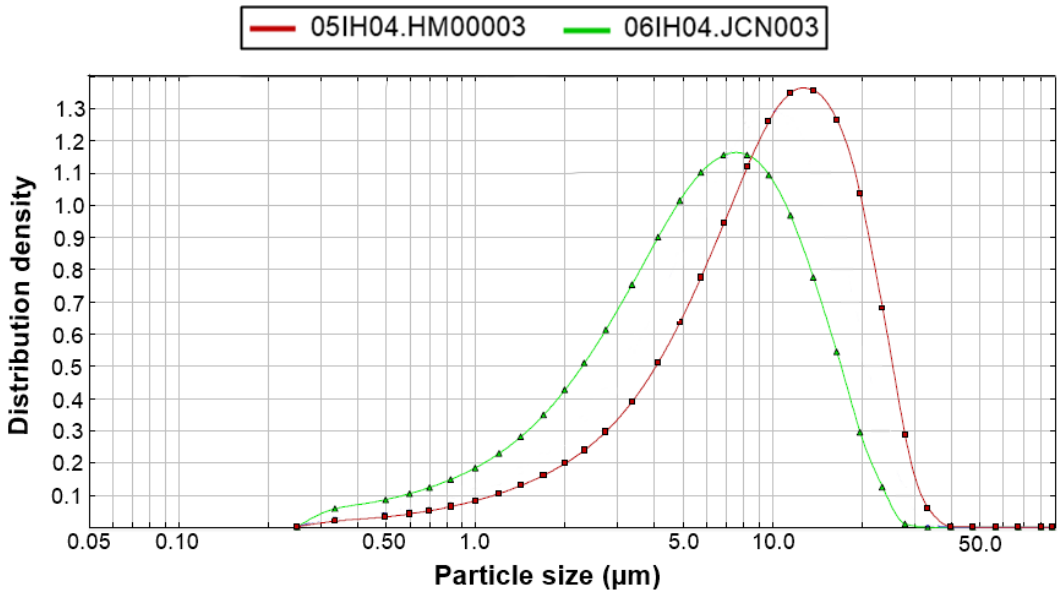

Figure 3.1: Particle size distribution of the SRMs 05IH04.HM00003 and 06IH04.JCN003.

Morphology

From the SEM images shown in Figure 3.2, it can be observed that the SRMs presented a plate-like morphology, as verified in literature[1]. Considering this morphology, the particle size measurements could be slightly misleading since the laser diffraction method assumes that all particles have a sphere-like shape [13]. Since the starting raw material 06IH04.JCN003 was obtained through manual grinding, smaller particles that could have been generated during this process were observed confirming the results obtained for PSD and span.

[1] Due to confidentiality, references will not be presented.

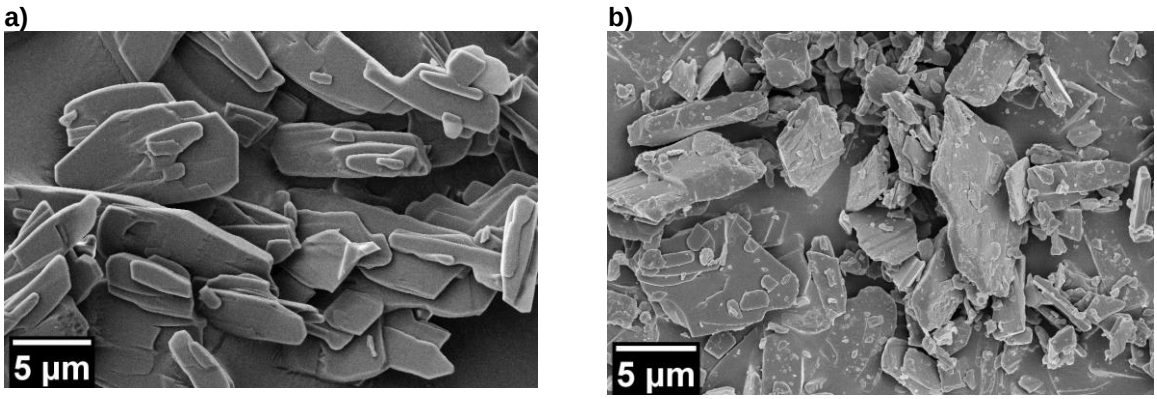

Figure 3.2: SEM images obtained at an ampliation of 2kX using an acceleration voltage of 5 kV of the SRMs a) 05IH04.HM00003 and b) 06IH04.JCN003.

Crystallinity, polymorphic form and crystallite size

The presence of peaks in the diffractograms presented in Figure 3.3 indicated that the two SRMs were crystalline, and presented the peaks characteristic of the most stable polymorphic form of IH04[1]. The manual grinding process did not affect the crystallinity nor the polymorphic form of the SRMs. Therefore, the increase of peak intensities observed for the SRM 06IH04.JCN003 in comparison with the SRM 05IH04.HM00003 may had been due to the variability of the measuring technique. Both SRMs presented similar CS; considering the Scherrer method for the CS calculation, the obtained CS was 29.6 nm and 28.8 nm for 05IH04.HM00003 and 06IH04.JCN003, respectively. Therefore, the manual grinding process did not affect the CS.

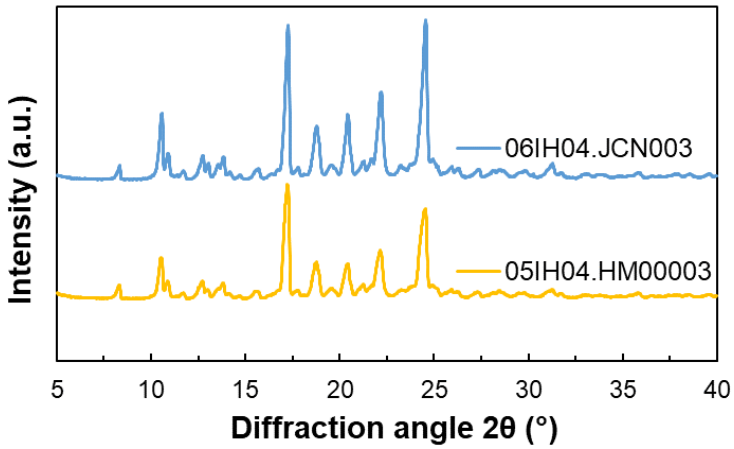

Figure 3.3: Diffractograms of the SRMs 05IH04.HM00003 and 06IH04.JCN003.

Nanoindentation

On Figure 3.4 is shown, as exemplificative, the indentation points made for one particle and one of the force-indentations tests that were performed for the SRM 05IH04.HM00003. The approach-retrace curves overlapped, meaning that the material presented a full elastic behavior as no plastic deformation occurred. The obtained hardness and Young modulus mean values for the SRM 05IH04.HM00003 were 320.00 ± 78.68 MPa and 253.30 ± 89.08 MPa, respectively. It was not possible to obtain reliable approach-retrace curves for the SRM 06IH04.JCN003. As erroneous approach-retrace curves, that were excluded, were also obtained for 05H04.HM00003, the variability of the results for the measuring technique suggested that nanoindentation by AFM may not be the most suitable technique for the measurement of these materials.

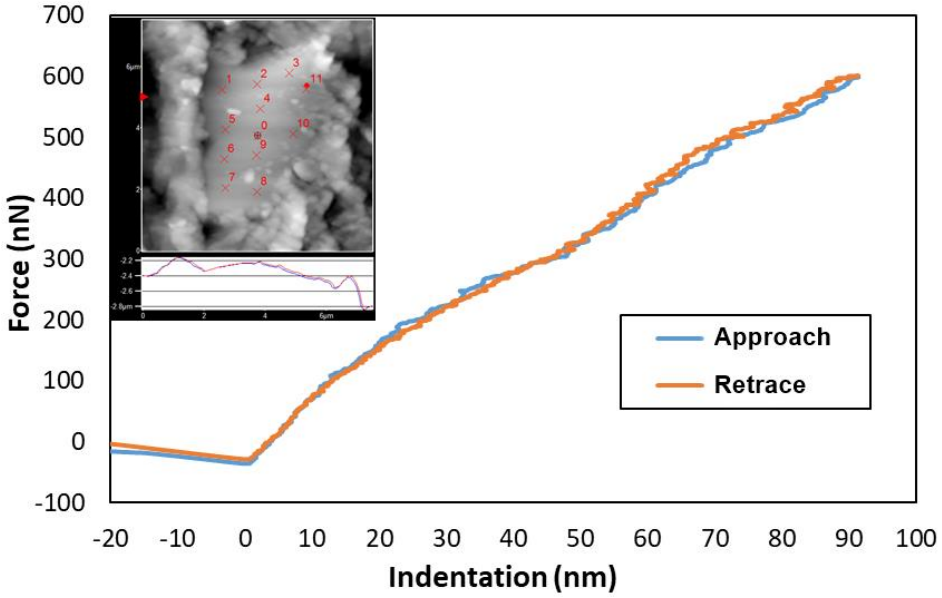

Figure 3.4: Surface scan of a particle of the SRM 05IH04.HM00003, showing the indentation points and a approach-retrace curve of one of the indentations performed.

From the Young modulus obtained for the SRM 05IH04.HM00003 (253.30 ± 89.08 MPa) and from the behavior observed from the approach-retrace curve it can be stated that this material presented an elastic behavior. Similar values of Young modulus were previously reported for elastic APIs [34] where materials having Young modulus of 50 MPa were considered to have elastic properties. However the value of hardness obtained (320.00 ± 78.68 MPa) indicated that 05IH04.HM00003 is considered to be a hard material as reported in literature by Chen et al. [52] where APIs with hardness of 430 MPa were considered to be hard materials.

As mentioned by Saleem et.al. [34], the mechanical properties of materials being milled have an important role in their final PSD. However, between hardness and Young modulus, the Young modulus was reported to be more critical [35] because plastic deformation is necessary for the fragmentation of particles. Since the SRM 05IH04.HM00003 is very elastic, it will require high energies to overcome its elastic properties and to reduce its PSD.

SSA, porosity, and density

Table 3.1 summarizes the obtained SSA, porosity (APD and TPV) and density values for the SRMs 05IH04.HM00003 and 06IH04.JCN003. Since the equipment error of measurement for SSA was 2.40 m^2/g, no relation was found between the two SRMs that presented SSA values which were close and even lower than the equipment error of measurement.

The APD results suggested that the SRMs were mesopore materials. Considering an equipment error of 0.10 nm and 0.004 cm^3/g for the APD and TPV, respectively, there was no significant variation of APD and TPV between the SRMs; only a small decrease of APD and TPV was observed for the SRM 06IH04.JCN003 when compared with the SRM 05IH04.HM00003. Although there was no significant variation of APD and TPV, the obtained density for 06IH04.JCN003 was higher than 05IH04.HM00003, which was expected since this material presented lower particle size. The Dv10 results already mentioned also supported this increase of density, as smaller particles that fill the empty spaces between larger particles were generated in the grinding process.

Table 3.1: SSA, porosity and density values of the SRMs 05IH04.HM00003 and 06IH04.JCN003.

Starting raw material	SSA (m^2/g)	APD (nm)	TPV (cm^3/g)	Density (g/cm^3 ± S.D.)
05IH04.HM003	2.91	16.99	0.012	1.050 ± 0.041
06IH04.JCN003	2.07	16.58	0.009	1.322 ± 0.016

3.2 Characterization of the micronized materials

The characterization of the micronized materials is divided in two sections. On the first section are shown the results obtained for the micronized materials using the SRM 05IH04.HM00003. On the second section a comparison between the micronized materials obtained from the SRMs 05IH04.HM00003 and 06IH04.JCN003 is presented.

The decision to divide the results in two sections was due to the number of experiments performed. For the SRM 06IH04.JCN003 only 4 experiments were performed due to the lack of time to complete the work.

All 16 micronized materials obtained from the SRM 05IH04.HM00003 were analysed on the first section in order to perform an analysis considering the Esp and the individual influence of the micronization process parameters (grinding pressure and feed rate), in order to have a better understanding of the material behavior during the micronization process. From the 16 micronized materials of 05IH04.HM00003, the four experiments with similar conditions as the ones performed with the SRM 06IH04.JCN003 were selected in order to make a comparison and study the influence of the SRM on the characteristics of the micronized materials.

3.2.1 Jet milling micronization using 05IH04.HM00003 as starting raw material

PSD

For the evaluation of the PSD, the graphics of Dv10, Dv50, and Dv90 of the micronized materials obtained from the SRM 05IH04.HM00003 were presented in Figure 3.5, and the respective values are also presented in Table 3.1. The particle size of the micronized materials decreased with the increase of Esp, as expected since a higher energy induced more particle-particle and particle-wall collisions [53]. When fitting a power regression of the results of Dv10, Dv50 and Dv90 as a function of Esp, it can be observed a poor fitting for Dv10 and a good fit for both Dv50 and Dv90. There is a rapid decrease of particle size at lower Esp values, reaching a plateau at approximately 0.60 µm, 1.60 µm, and 3.40 µm for Dv10, Dv50 and Dv90. There were two samples points that deviated from the regression lines of Dv10, Dv50, and Dv90; these samples were considered outliers and were excluded.

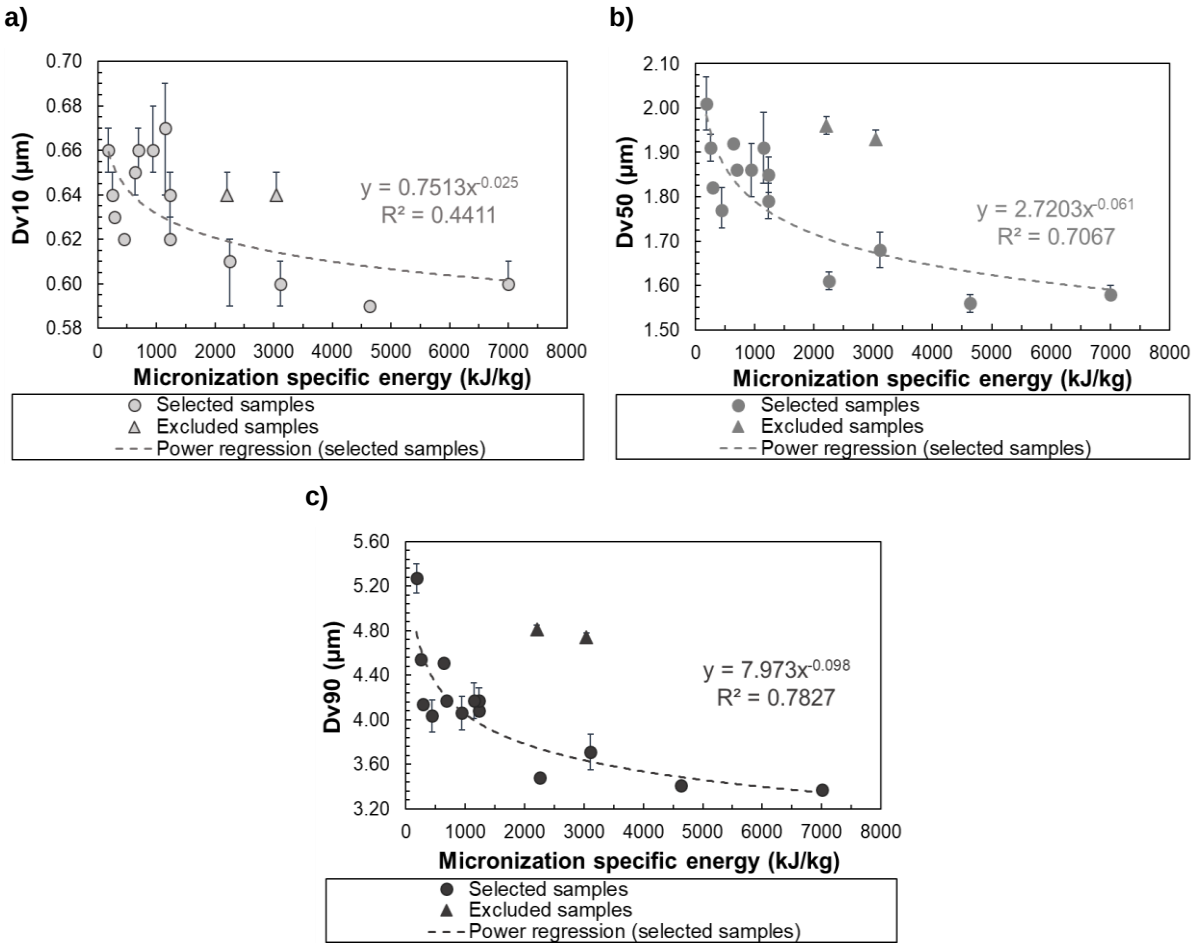

Figure 3.5: Effect of the increase of Esp during the micronization process on the calculated a) Dv10, b) Dv50 and c) Dv90 average values (n=3) of the micronized materials from the SRM 05IH04.HM00003.

Table 3.1: PSD and span of the SRM 05IH04.HM00003 and the materials micronized with the respective Esp value.

	Esp (kJ/kg)	Average Dv10 (µm)	Average Dv50 (µm)	Average Dv90 (µm)	Span
Starting raw material (05IH04.HM00003)	-	2.08	8.93	19.20	1.78
Micronized materials	180.31	0.66	2.01	5.27	2.29
	252.06	0.64	1.91	4.54	2.04
	290.01	0.63	1.82	4.14	1.93
	443.76	0.62	1.77	4.04	1.93
	634.98	0.65	1.92	4.51	2.01
	689.20	0.66	1.86	4.17	1.89
	944.23	0.66	1.86	4.06	1.83
	1148.07	0.67	1.91	4.17	1.83
	1231.37	0.62	1.79	4.08	1.93
	1232.82	0.64	1.85	4.17	1.91
	2207.79	0.64	1.96	4.81	2.13
	2252.07	0.61	1.61	3.48	1.78
	3043.45	0.64	1.93	4.74	2.12
	3111.68	0.60	1.68	3.71	1.85
	4632.27	0.59	1.56	3.41	1.81
	7003.20	0.60	1.58	3.37	1.75

A further analysis was performed by considering the individual influence of the micronization process parameters, in order to have a better understanding of the material behavior during the micronization process. For this purpose, the results were grouped considering a constant grinding pressure, and feed rate intervals. To group the micronized samples by means of feed rate, four proximity intervals were created. Figure A.1, Figure A.2 and Figure A.3 in Appendix A shows the Dv10, Dv50, and Dv90, respectively, of the micronized materials from the SRM 05IH04.HM00003, where each series correspond to a constant value of grinding pressure and feed rate intervals.

Considering the micronized materials from the SRM 05IH04.HM00003, grouped by a constant grinding pressure, it could be observed that the Dv10, Dv50 and Dv90 decreased with the increase of Esp, being the stronger correlations obtained for Dv90. It can also be observed that for the same values of Esp, a change on the pressure led to a considerable change on the Dv10, Dv50 and Dv90.

When grouping by feed rate intervals, a linear regression fitted well the results of Dv10, Dv50 and Dv90 and it was observed a decrease of these parameters with the increase of Esp. However, for the same values of Esp the variation of the feed rate led only to small changes on the PSD, contrary to what was observed for the grinding pressure. This was an indicator that the grinding pressure had a higher influence on the PSD than the feed rate.

The results for grinding pressure and feed rate were expected and are in accordance with literature; higher grinding pressures led to higher velocities of the spiral vortex created in the grinding chamber, which is reflected on higher kinetic energy and consequently more collisions between particles [26, 54]. It is also known that, for lower feed rates, more energy is available for each particle, which resulted in a more efficient breakage between them [34].

The relation between span and Esp followed a power regression, as presented in Figure 3.6, were no error bars were presented as only the average value of each PSD parameterwere directly obtained using the Sympatec software. The span measurements may also be observed in the previously mentioned Table 3.1. Span is an indicator of PSD, therefore lower span values indicated that narrower PSD was obtained at higher Esp values, which is related to a better homogenization of particle size [54]. Considering the PSD results of the micronized materials from the SRM 05IH04.HM00003, the percentage of the decrease of Dv10, Dv50 and Dv90 as a function of Esp was calculated. The decrease on Dv10 was between 1% and 11%, for Dv50 was between 2% and 23%, and for D90 was between 8% and 37%.

As Dv90 presented the highest variation and considering equation (2.2), it is possible to conclude that this fast decrease of Dv90 led to lower span values. The same outliers observed for Dv10, Dv50 and Dv90 were identified and excluded for the regression.

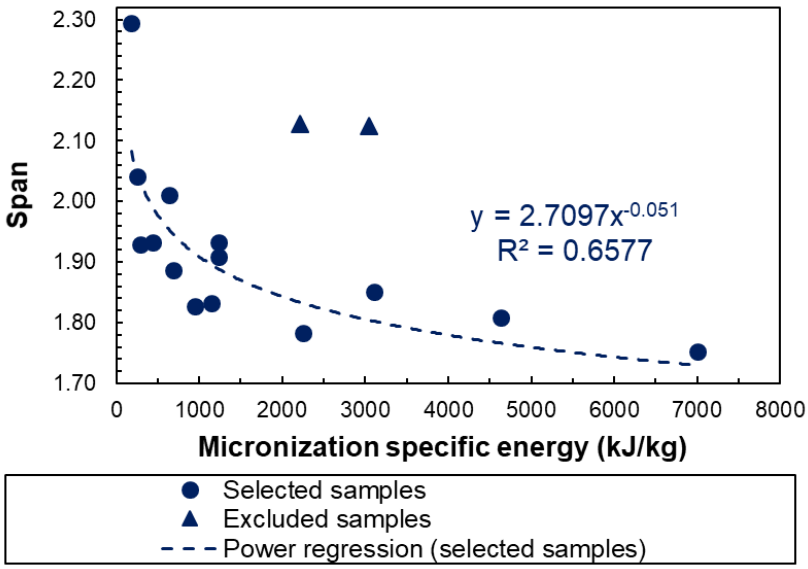

Figure 3.6: Effect of the increase of Esp during the micronization process on the calculated span of the micronized materials from the SRM 05IH04.HM00003

The span values of the micronized materials from the SRM 05IH04.HM00003 were grouped considering a constant grinding pressure and feed rate intervals, as observed in Figure A.4 in Appendix A. Grouping by grinding pressure, good relations represented by power regressions were observed for grinding pressures of 2 bar, 4 bar and 6.5 bar, as the span decreased with the increase of Esp. No relation was verified for the micronized materials micronized at grinding pressures of 5.5 bar However, it can be observed that the variation of grinding pressure led to a change of span, considering a constant Esp value.

When grouping in feed rate intervals, a decrease of span with the increase of Esp between the span and Esp was observed for the feed rate intervals of 4.65 g/h - 7.03 g/h and 63.60 g/h - 112.29 g/h presenting a fitted linear regression, whereas no relation for feed rate intervals of 9.07 g/h - 18.91 g/h and 22.92 g/h - 40.95 g/h was observed. Therefore, no relation between the span and the feed rate was observed. Considering these results, it can be concluded that the grinding pressure influenced more the span values of the micronized materials than the feed rate.

Morphology

The SEM images of the micronized materials from the SRM 05IH04.HM00003 which were labelled by the correspondent micronization Esp are presented in Figure 3.7. As it can be observed, the morphology did not change with the increase of the micronization Esp, a plate-like morphology was observed for all the micronized materials[1]. These results were good since it was observed that a change in morphology of the APIs could compromise the aerosolization process [55], being crucial for the performance of DPIs.

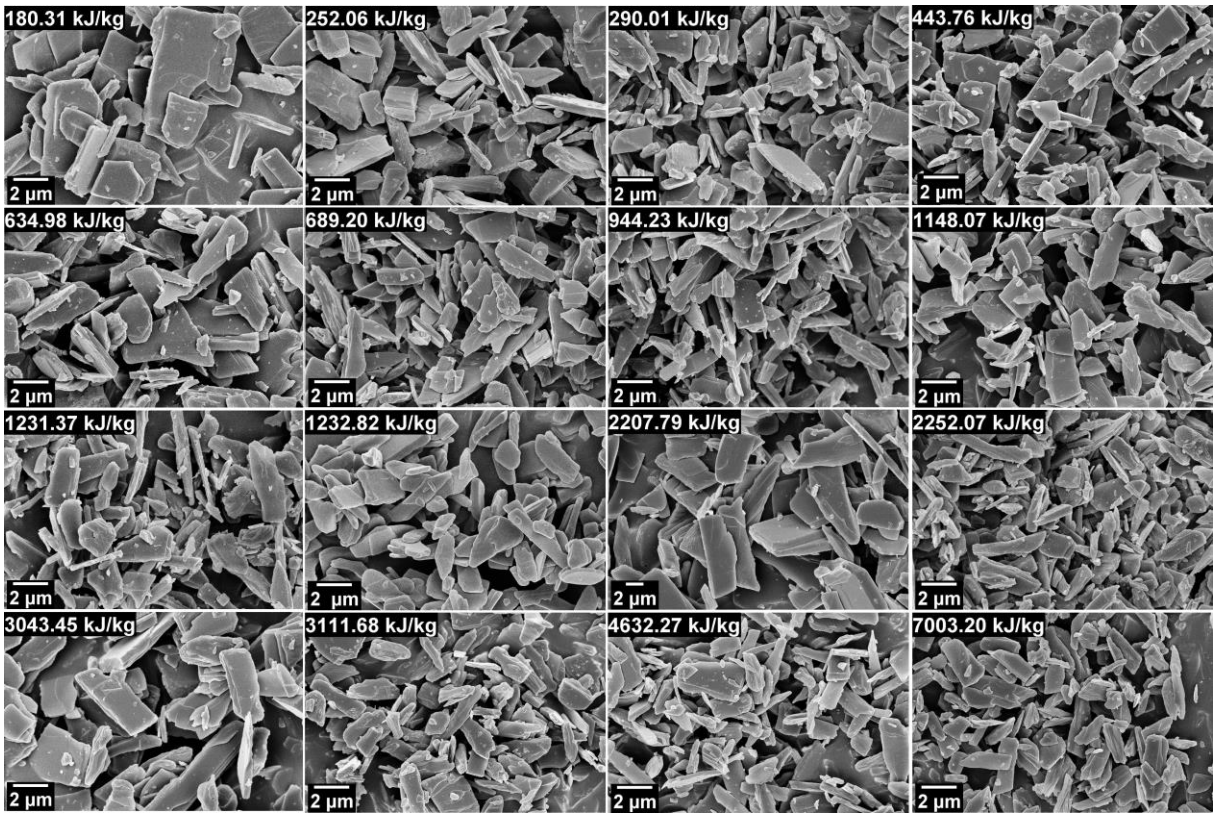

Figure 3.7: SEM images obtained at an ampliation of 5kX of the micronized materials 06IH04M.JCN005 to 06IH04M.JCN0020 from the SRM 05IH04.HM00003 and identified by their respective Esp value.

Crystallinity, polymorphic form and crystallite size

As previously stated, the samples were stored in cold conditions so no recrystallization of the material could occur after the JM process. The XRD diffractogram of the micronized materials for the SRM 05IH04.HM00003 is presented in Figure 3.8. As observed, the micronized materials kept the same stable polymorphic form of the SRM. It must be stated that different polymorphic forms may present different physicochemical properties that could affect the final formulation performance [18, 57]. It is well known that milling processes could lead to an amorphization of the micronized materials [19, 47], that would lead a lower crystallinity of the obtained materials. However, it was observed that, with exception of the material micronized with an Esp of 180.31 kJ/kg that showed higher peaks intensities, showed similar crystallinity between each other and with the SRM.

As no relation between the crystallinity of the micronized materials and the Esp was observed, the higher peaks intensities observed for the material micronized at 180.31 kJ/kg may be explained by the variability of the measuring method, or by an experimental error during the measurement. A small peak shift for the micronized material obtained at an Esp of 290.01 kJ/kg that may have been caused by poor-quality sample preparation was also be observed.

Despite all the micronized materials were already crystalline even if stored at cold conditions, in order to investigate if there was still occurring any recrystallization process, it was decided to store sample 06IH04M.JCN008 at room conditions (T=25ºC and a RH=50%) during 1 week and to perform the XRD measurement again. As shown in Figure 3.9, the diffractograms were very similar meaning that no recrystallization occurred and that the product has no amorphous content after the JM process.

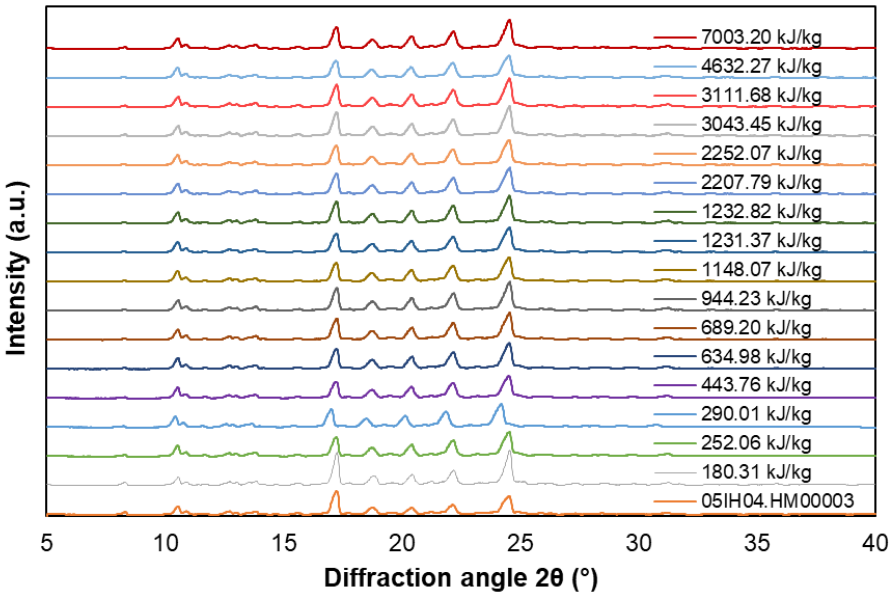

Figure 3.8: Diffractograms of the SRM 05IH04.HM00003 and the micronized materials with their respective Esp.

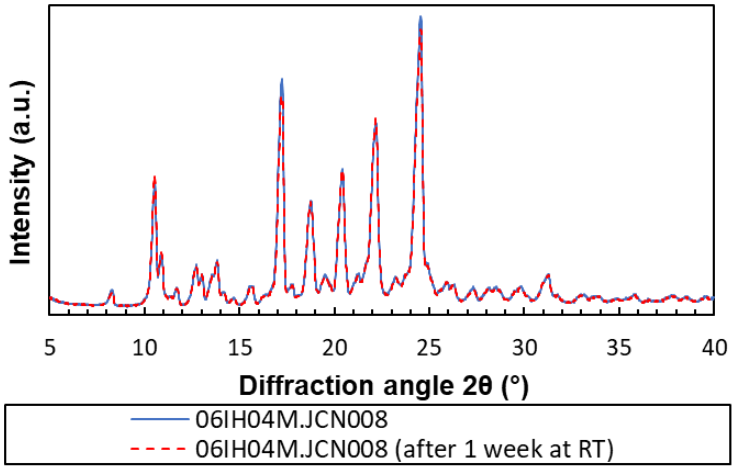

Figure 3.9: Diffractograms of samples of the micronized materials from 06IH04M.JCN008 in storage at low temperatures, and after 1 week at room conditions.

As shown in Figure 3.10, it is possible to observe a tendency of the CS to decrease with the increase of Esp. These results may be explained by making a comparison with a previous work where a different type of milling equipment was used, where the CS decreased and reached a plateau, that was related to the equilibrium between the recrystallization of small amorphous fractions in the milled material and the fragmentation process [58].

Therefore, as a poor relation between crystallinity and Esp was observed in the XRD diffractogram previously presented, these results suggest that an equilibrium between the fragmentation process and the recrystallization of small amorphous fractions never occurred with the change of Esp. No error bars were shown as only one measurement of the CS for each micronized material was performed.

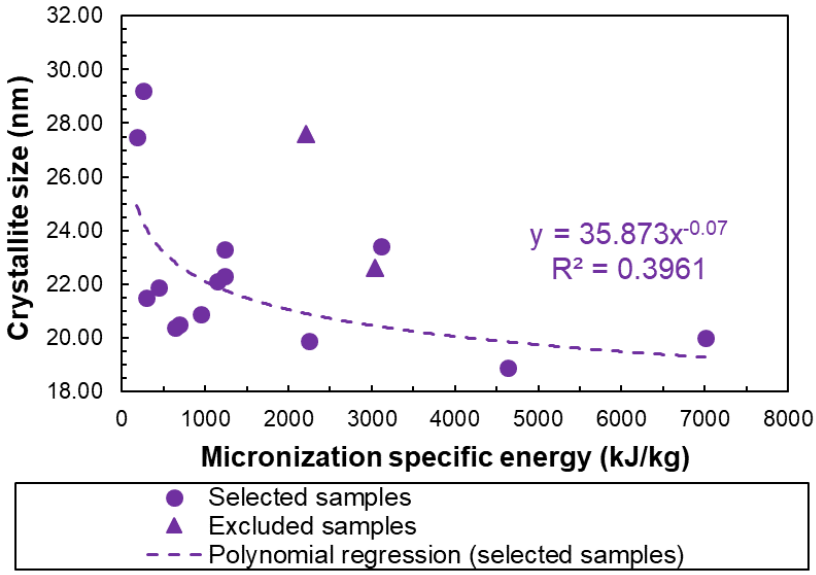

Figure 3.10: Effect of the increase of Esp during the micronization process on the calculated CS of the micronized materials from the SRM 05IH04.HM00003.

In Figure A.5 in Appendix A, the individual influence of the CS as a function of Esp considering a constant grinding pressure and feed rate intervals is presented. For a constant grinding pressure, a relation between the CS and the Esp was only observed for grinding pressures of 4 bar and 6.5 bar, that presented a fitted power regression. However, for a pressure of 2 bar and 5.5 bar no relation was observed.

Regarding the individual influence of the feed rate, it was observed an increase of the CS with the Esp for the materials micronized within a feed rate interval of 22.92 g/h - 40.95 g/h and 9.07 – 18.91 g/h, contrary to the decrease observed for the material micronized within the feed rate interval of 4.65 g/h - 7.03 g/h and 63.60 g/h - 112.29 g/h. Contrary to what was observed for the PSD, it was not possible to stablish a relation between the CS and the pressure and feed rate parameters individually since no linear correlation was found for the different intervals of both pressure and feed rate.

Specific Surface area

Regarding the SSA and considering an equipment error of 2.40 m²/g for the measurements, on Figure 3.11 it can be observed that a polynomial regression correlates the SSA with the Esp. A rapid increase of SSA was observed for Esp values lower than 2500 kJ/kg; however, for higher Esp values a decrease of SSA was also verified.

The same behavior was already reported by Nakach et al. [21]; the existence of two micronization regimes was stated, where the decrease of particle size was mainly due to fragmentation and attrition at lower and higher Esp values, respectively. Materials milled at higher Esp underwent micronization in the attrition regime, suffering a surface amorphization in the process and a rearranged upon storage at room temperature, lowering the SSA. However, since the micronized materials in this work were stored at low temperatures, and as observed from the XRD characterization the material has no amorphous content after the JM process, a possible explanation for this behavior would be that surface amorphization could have occurred during milling process, followed by a rapid surface rearrangement before storage.

This unstable behavior is not desired since the change of SSA, or any material property could lead to different drug performance [18, 39]. Therefore, micronizations performed on the fragmentation regime at lower Esp are preferred to obtain stable micronized materials, which was also referred by Nakach et al. (2019).

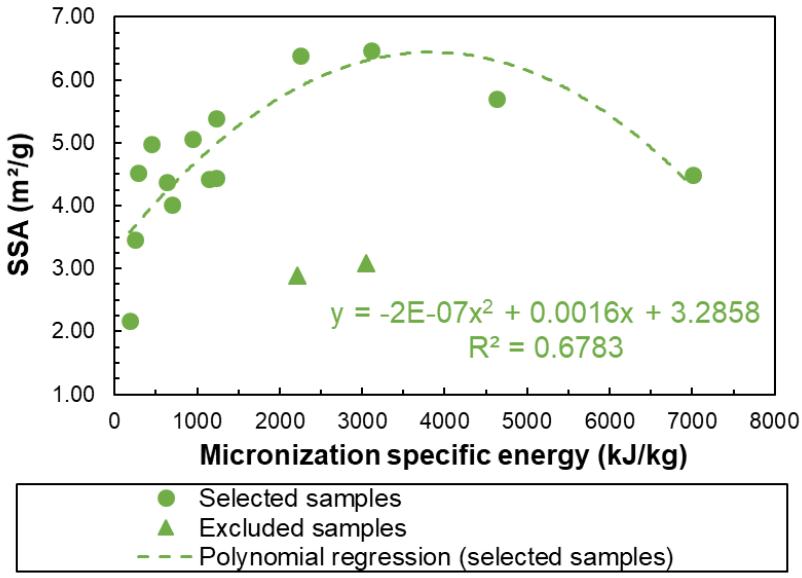

Figure 3.11: Effect of the increase of Esp during the micronization process on the calculated SSA of the micronized materials from the SRM 05IH04.HM00003.

A representation of the results by different series of data with constant grinding pressure and feed rate intervals as a function of Esp is presented in Figure A.6 in Appendix A.

For an analysis considering a constant grinding pressure, the two regimes mentioned before were considered. In the fragmentation regime at Esp values < 2500 kJ/kg, it was possible to observe an increase of SSA with the increase of Esp, represented by power regressions for the micronized materials regarding grinding pressures of 2 bar, 4 bar and 5.5 bar; a with a polynomial regression for the micronized materials for a constant grinding pressure of 6.5 bar. It was possibly to observe that for a constant Esp, the increase of grinding pressure led to an increase of the SSA of the micronized materials. For the attrition regime at higher Esp values, it was not possible to observe this relation pressure, as only a decrease of SSA for a constant grinding pressure of 6.5 bar was verified.

For the fragmentation regime at Esp values < 2500 kJ/kg, it was only possible to observe an increase of SSA with the increase of Esp for the feed rate intervals of 9.07 g/h - 18.91 g/h, 22.92 g/h - 40.95 g/h and 63.60 g/h - 112.29 g/h, that followed a linear regression. For the attrition regime at higher Esp values, only a poor relation between SSA and Esp was observed for the micronized materials for the feed rate interval of 4.65 g/h - 7.03 g/h.

For the fragmentation regime it can also be observed that, for the same values of Esp, led only to small changes of SSA, when compared with the results considering a constant grinding pressure, which suggested that the grinding pressure influenced more the SSA of the micronized materials than the feed rate. It must be stated that the equipment error of measurement is relatively high (2.40 m^2/g) and may have had a considerable impact on the deviation of the samples from their respective regression, as observed for the SSA of the materials micronized at a constant grinding pressure of 5.5 bar.

Porosity

Figure 3.12 shows a representation of the APD as a function of Esp for the materials micronized from the SRM 05IH04.HM00003. The results suggested that the micronized materials contained mesopores. A weak relation between APD and Esp was obtained as it can be observed from the power regression. These results may be explained by the two regimes previously mentioned and reported by Nakach et al. [21]. For Esp values lower than 2500 kJ/kg, in the fragmentation regime, different APD values were obtained for similar Esp values, suggesting that non-uniform pores sizes were formed when the breakage of particles was mainly due to fragmentation. For higher Esp values, in the attrition regime, more uniform pores were formed as the APD remained almost constant at approximately 9 nm, presenting only a minimal variation with the increase of Esp.

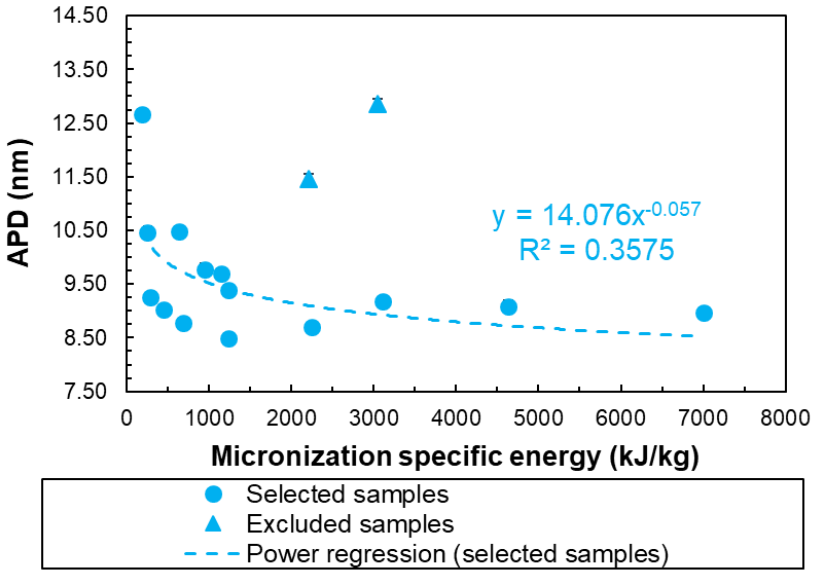

Figure 3.12: Effect of the increase of Esp during the micronization process on the calculated APD of the micronized materials from the SRM 05IH04.HM00003.

Analysing the micronized samples considering the individual influence of the micronization process parameters (grinding pressure and feed rate), as presented in Figure A.7 in Appendix A, no relation between APD and Esp was observed for the materials micronized at a constant grinding pressure of 2 bar, 5.5 bar and 6.5 bar; only a moderate relation was observed the micronized materials regarding a grinding pressure of 4 bar, showing a decrease of APD with the increase of Esp. Therefore, it was not possible to stablish a common relation of the change of APD with the increase of grinding pressure.

Similar results were observed when the micronized materials were grouped by means of feed rate intervals. A decrease of APD of the micronized materials with the increase of Esp was only observed for the feed rate intervals of 4.65 g/h - 7.03 g/h and 63.60 g/h - 112.29 g/h, whereas no relation between APD and Esp was observed for the feed rate intervals of 9.07 g/h - 18.91 g/h and 22.92 g/h - 40.95 g/h.

Therefore, no relation was observed between the APD and the grinding process parameters individually since no linear correlation was found for the different intervals of both pressure and feed rate.

The TPV, as a function of Esp, is presented in Figure 3.13, considering an error of equipment for the measurements of 0.004 cm^3/g. Similar behavior as for the SSA as a function of Esp was observed which was expected since both parameters are highly correlated [22]. The TPV results followed a polynomial relation with the increase of Esp, increasing for lower values of Esp and decreasing for higher values of Esp. These results could again be explained by the two existent regimes that could occur on the JM micronization process, fragmentation and attrition. A rapid increase of TPV occurred at lower Esp values in the fragmentation regime. In the attrition regime; the surface amorphization that could have occurred during the milling process, followed by a rapid surface rearrangement, may have led to a decrease of TPV.

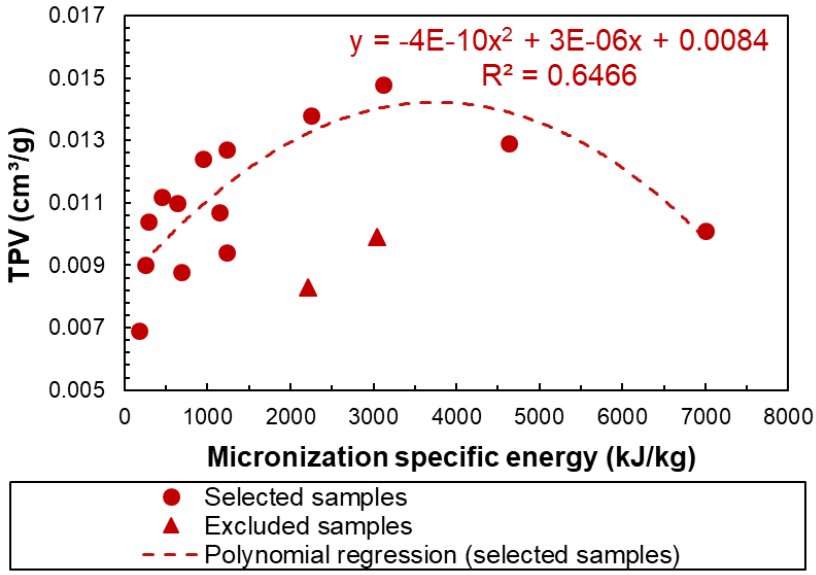

Figure 3.13: Effect of the increase of Esp during the micronization process on the calculated TPV of the micronized materials from the SRM 05IH04.HM00003.

The individual influence of the micronization process parameters grinding pressure and feed rate was studied by grouping the micronized materials by means of grinding pressure and feed rate intervals, as presented in Figure A.8 in Appendix A. The two micronization regimes were also considered.

For the micronized materials grouped by considering a constant grinding pressure, an increase of TPV with the increase of Esp was observed for grinding pressures of 2 bar, 5.5 bar and 6.5 bar. No relation between TPV and Esp was observed for the materials micronized at a grinding pressure of 4 bar. Similar relation as for the SSA was observed, as the variation of grinding pressure led to a change of TPV, when a constant Esp was considered.

Similarly, as for the SSA, an increase of TPV with the increase of Esp was only observed for feed rate intervals of 9.07 g/h - 18.91 g/h, 22.92 g/h - 40.95 g/h and 63.60 g/h - 112.29 g/h, whereas no relation between TPV and Esp was observed for the feed rate interval of 4.65 g/h - 7.03 g/h, that was mainly in the attrition regime at higher Esp values. Regarding the fragmentation regime, small changes of TPV were observed when the variation of the feed rate when compared with the variation of grinding pressure. Therefore, the grinding pressure influenced more the TPV.

The equipment error of measurement should also be considered (0.004 cm^3/g), as its magnitude is closer the performed measurements of the micronized materials. Thus, it could have influenced the results.

Density

As shown in Figure 3.14, no relation between the density of the micronized materials and Esp was observed. This relation was not expected, as the decrease of particle size by milling was already performed to increase the density of the micronized materials in previous works [60, 61] in order to improve properties such as solubility. It was also stated that density was referred as a crucial SRM property that affects micronized material characteristics such as particle size and crystal structure [21].

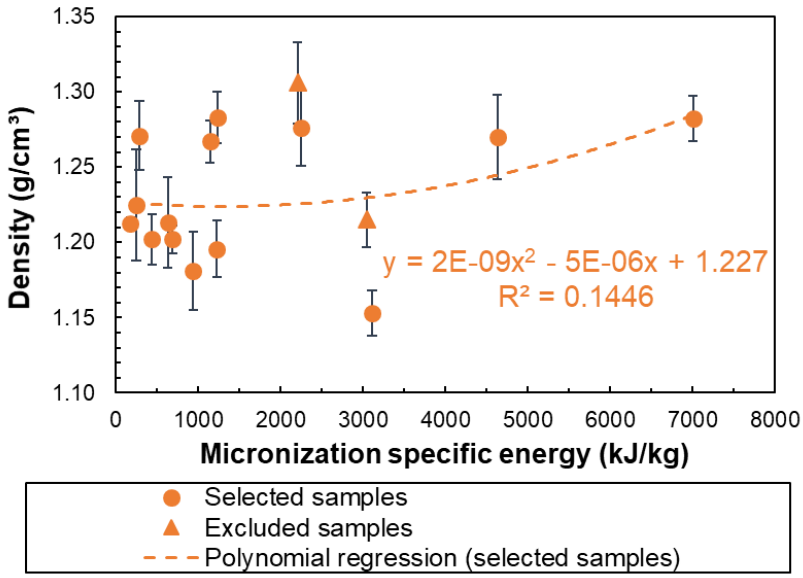

Figure 3.14: Effect of the increase of Esp during the micronization process on the calculated density of the micronized materials from the SRM 05IH04.HM00003.

Analysing the micronized materials by means of grinding pressure, as observed in Figure A.9 in Appendix A, it was only possible to observe a relation between density and Esp for a constant grinding pressure of 4 bar and 5.5 bar. However, these relations were different; an increase of density with the increase of Esp was observed for a constant grinding pressure of 4 bar, whereas a constant grinding pressure of 5.5 bar showed a decrease of density with the increase of Esp.

Considering the micronized materials grouped by a feed rate interval, the only relation observed was for the feed rate interval of 22.92 g/h - 40.95 g/h, that presented a decrease of density with the increase of Esp. Considering these results, it was not possible to stablish a relation between density with the variation of the grinding pressure and feed rate, since no correlation was observed with their variation.

3.2.2 Comparison of the micronized materials from 05IH04.HM00003 and 06IH04.JCN003 as starting raw materials

Due to time constrains, only four micronized materials with different micronization conditions were obtained from the SRM 06IH04.JCN003; thus, it was not possible perform an exhaustive study as for the SRM 05IH04.HM00003. However, a comparison was made for the micronized materials obtained from the SRMs 05IH04.HM00003 and 06IH04.JCN003 that were micronized with similar micronization conditions.

PSD

A comparison of Dv10, Dv50, and Dv90 as a function of Esp for the micronized materials obtained from the SRMs 05IH04.HM00003 and 06IH04.JCN003 is presented in Figure 3.15. For Dv90, the micronized materials from both SRMs followed and were well explained by a power regression, presenting a strong relation. A decrease of Dv90 with the increase of Esp was verified, that reached a plateau at approximately 3.40 µm at higher Esp values for the micronized materials from both SRMs. Only a slightly smaller Dv90 was observed for the micronized materials obtained from the SRM 06IH04.JCN003 when compared with the micronized materials from the SRM 05IH04.HM00003.

A similar but weaker relation as for Dv90 was observed for the obtained Dv50 of the micronized materials from both SRMs. The Dv50 of the micronized materials from the SRM 06IH04.JCN003 were slightly smaller than those from the SRM 05IH04.HM00003; the Dv50 also reached a plateau of 1.60 µm at higher Esp values for the micronized materials of both SRMs.

An even weaker relation was observed for the decrease of Dv10 of the micronized materials from the SRM 05IH04.HM00003 with the increase of Esp. However, no relation of Dv10 with the change of Esp was observed for the micronized materials from the SRM 06IH04.JCN003.

Therefore, these results suggest that the particle size of the SRMs did not affect significantly the obtained Dv10, Dv50 and Dv90 of the micronized materials.

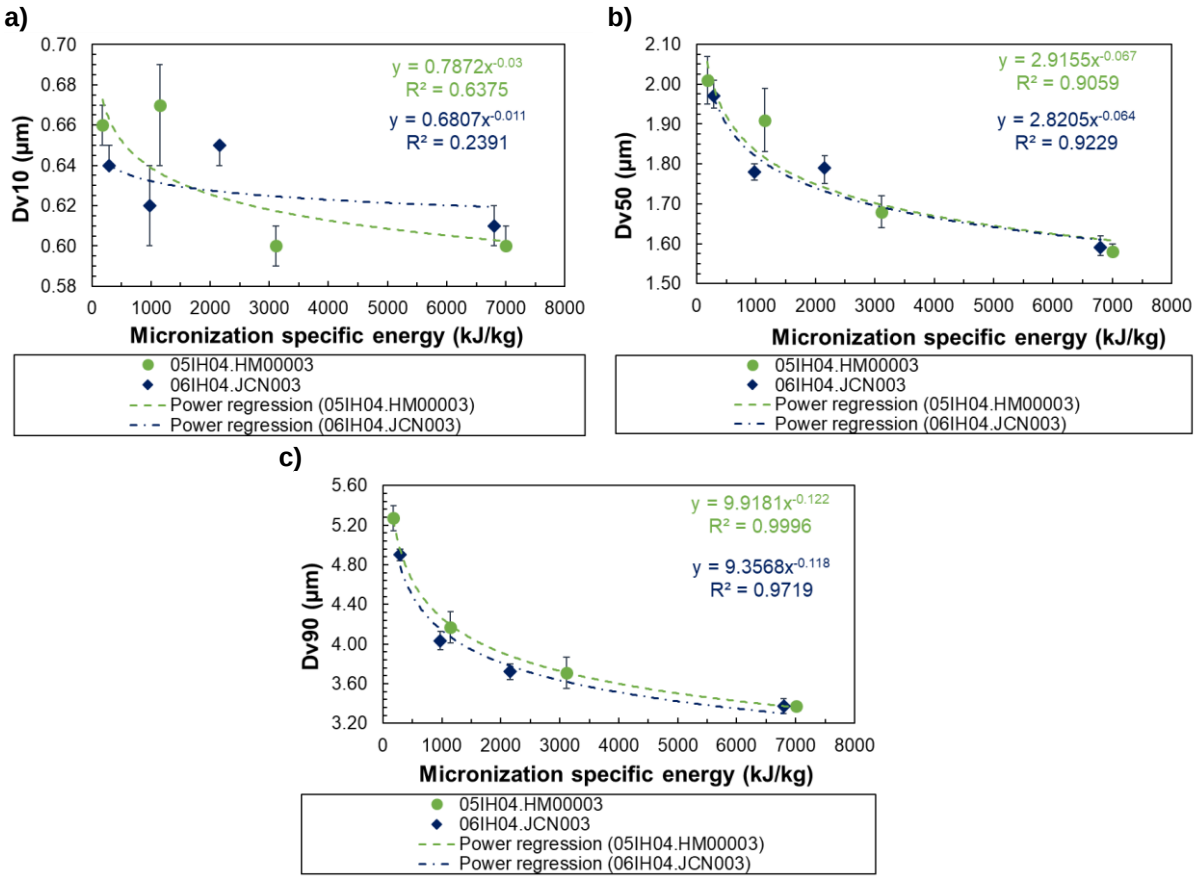

Figure 3.15: Dv10, Dv50 and Dv90 as a function of Esp for the micronized materials from the SRMs 05IH04.HM00003 and 06IH04.JCN003.

As shown in Figure 3.16, a power regression fitted well the decrease of span with the increase of Esp for all the micronized materials obtained from different SRMs meaning that for higher Esp it was possible to obtain a better homogenization of particle size [54]. Similar to what was observed on the previous subchapter, the main parameter of influence is Dv90 that had a maximum variation of 44% while Dv10 and Dv50 had a smaller variation of 10% and 22% respectively.

Comparing the span values of the micronized materials for both SRMs, no relation was observed for the span with the decrease of particle size of the SRMs. Therefore, the variation of the particle size for the SRMs did not affect the span of micronized materials.

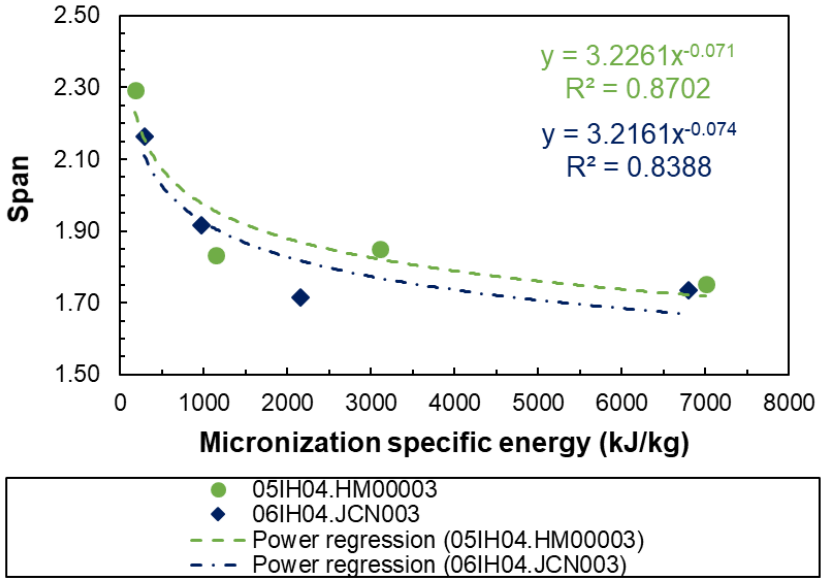

Figure 3.16: Span as a function of Esp of the micronized materials from the SRMs 05IH04.HM00003 and 06IH04.JCN003.

Morphology

The SEM images of the micronized materials from the SRMs 05IH04.HM00003 and 06IH04.JCN003 are presented in Figure 3.17. Despite using SRMs with different particle size, the same plate-like morphology was observed for all the micronized materials. Therefore, these results suggested that a different initial particle size did not have an influence on the morphology of the micronized materials.

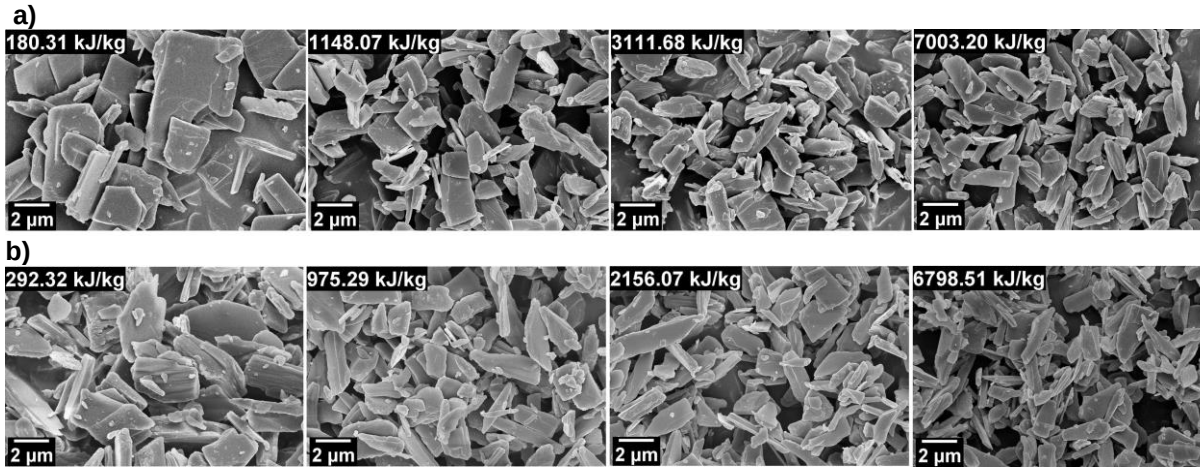

Figure 3.17: SEM images obtained at an ampliation of 5kX of the micronized materials from the SRMs a) 05IH04.HM00003 and b) 06IH04.JCN003 and identified by their respective Esp value.

Crystallinity, polymorphic form, and crystallite size

Figure 3.18 shows the diffractograms of the micronized materials for the SRMs 05IH04.HM00003 and 06IH04.JCN003. The same stable polymorphic form as for the SRMs was identified for all the micronized materials. Thus, the variation of the particle size of the SRMs did not affect their polymorphic form. It can be observed that the micronized materials obtained from the SRM with the largest PSD (05IH04.HM00003) were more crystalline while those obtained with the SRM with a lowest PSD (06IH04.JCN003) were less crystalline. For higher Esp values, similar peak intensities were observed for the materials micronized from the different SRMs, meaning that no amorphization occurred as their crystallinity did not change with the increase of Esp.

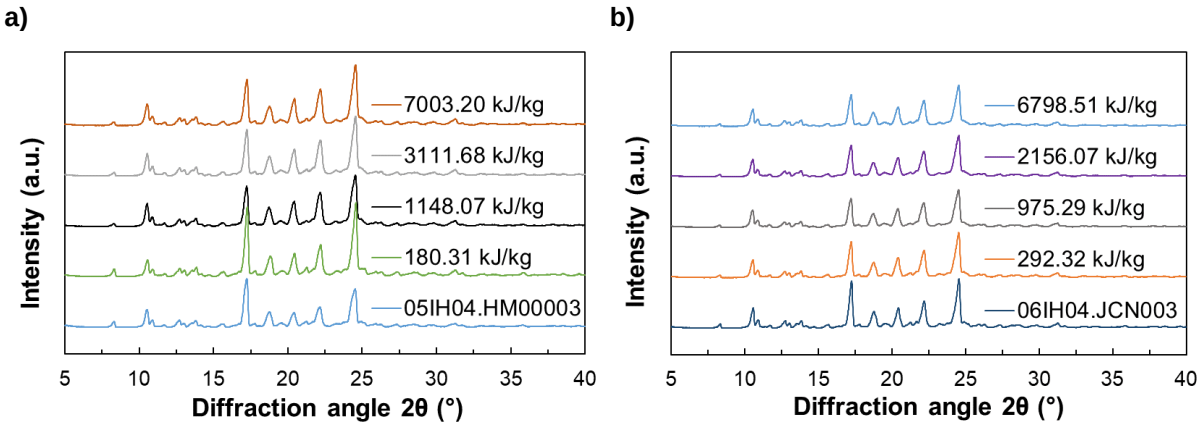

Figure 3.18: Diffractograms for the micronized materials from the SRMs a) 05IH04.HM00003 and b) 06IH04.JCN003.

The relation between CS and Esp regarding the micronized materials from the SRMs 05IH04.HM00003 and 06IH04.JCN003 is presented in Figure 3.19. A decrease of CS with the increase of Esp was observed for the micronized materials from the SRMs 05IH04.HM00003 and 06IH04.JCN003. The difference on the particle size of the SRMs did not influence the results, as no clear relation was verified when comparing the micronized material obtained from each SRM.

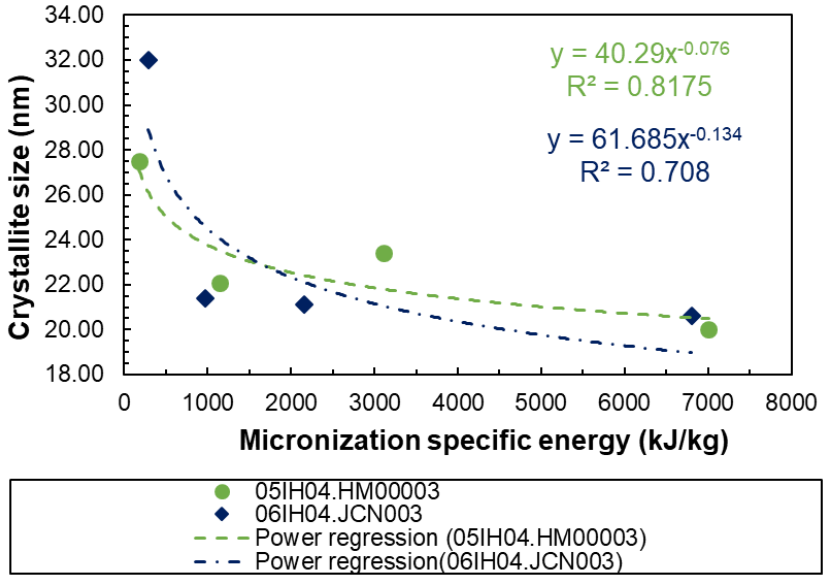

Figure 3.19: CS as a function of Esp of the micronized materials from the SRMs 05IH04.HM00003 and 06IH04.JCN003.

Specific Surface area

Analysing the SSA as a function of Esp for the micronized materials obtained from the SRMs 05IH04.HM00003 and 06IH04.JCN003, as shown in Figure 3.20, it was possible to observe that micronized materials with higher SSA were obtained from the SRM 06IH04.JCN003 when compared with the micronized materials for the SRM 05IH04.HM00003, which suggested that a decrease of the particle size of the SRM led to an increase of the SSA of the micronized materials.

The same behavior observed in the previous sub-chapter for the SSA characterization of the micronized materials regarding the SRM 05IH04.HM00003 was also verified for the SRM 06IH04.JCN003; which suggested that at higher Esp values, in the attrition regime, the micronized materials from the SRM

06IH04.JCN003 suffered a surface amorphization during the milling process [21], followed by a quick surface rearrangement that could have led to a decrease of SSA.

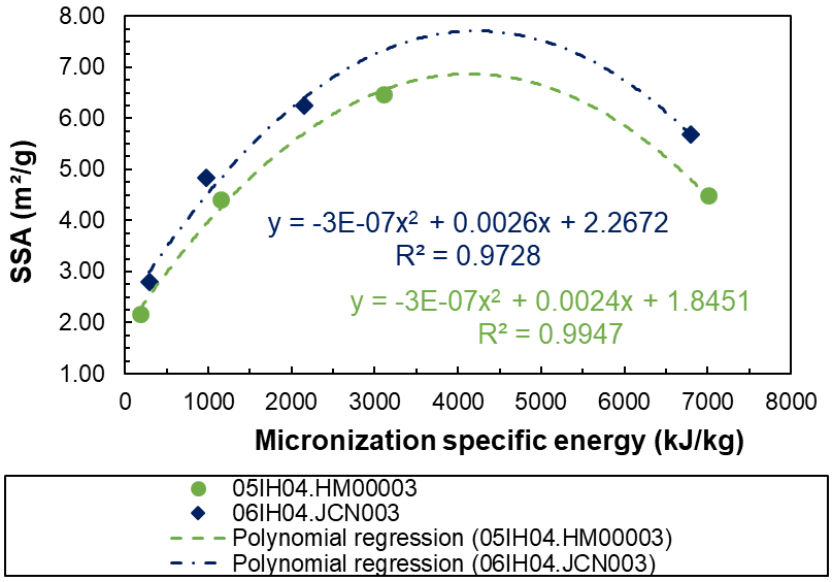

Figure 3.20: SSA as a function of Esp of the micronized materials from the SRMs 05IH04.HM00003 and 06IH04.JCN003.

Porosity

Figure 3.21 shows the variation of the APD with the Esp for the micronized materials obtained from the SRMs 05IH04.HM00003 and 06IH04.JCN003. No relation was observed between the APD of the micronized materials and the variation of the particle size of the SRMs.

For Esp values lower than 2500 kJ/kg, in the fragmentation regime, a decrease of APD with the increase of Esp was observed for all the micronized materials. For higher Esp values, in the attrition regime, the micronized materials of the SRM 05IH04.HM00003 presented only a small variation of APD; whereas the micronized materials of the SRM 06IH04.JCN003 presented a slight increase in APD, which may not be significative.

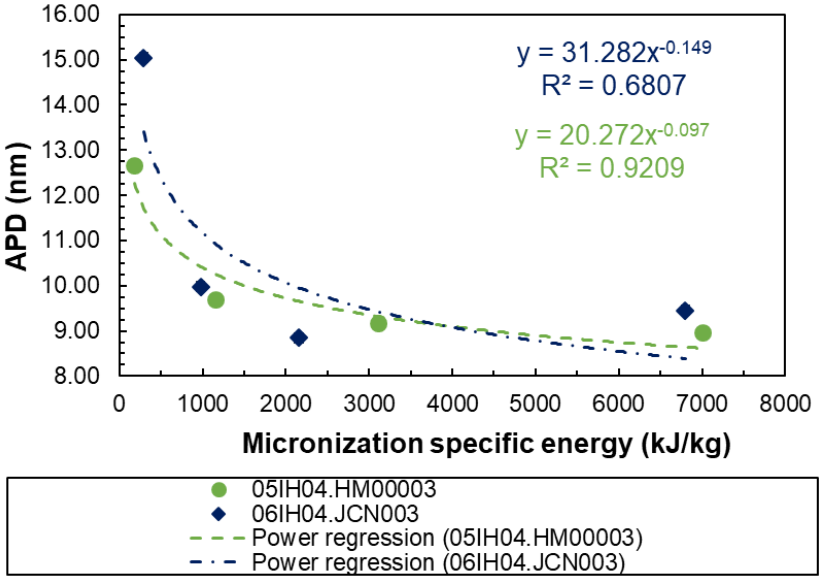

Figure 3.21: APD as a function of Esp of the micronized materials from the SRMs 05IH04.HM00003 and 06IH04.JCN003.

The TPV of the micronized materials for each SRM as a function of Esp is presented in Figure 3.22. It was observed that micronized materials obtained by SRMs with lower particle size (06IH04.JCN003) presented higher TPV values than micronized materials obtained by milling SRMs with higher particle size (05IH04.HM00003).

Similar behavior as for the SSA results was observed for TPV, which was expected considering the linear correlation between these parameters [22]. Therefore, the decrease of TPV in the attrition regime for the micronized materials from the SRM 06IH04.JCN003 may also be related to the surface amorphization that could have occurred during the milling process, followed by a rapid surface rearrangement before storage.

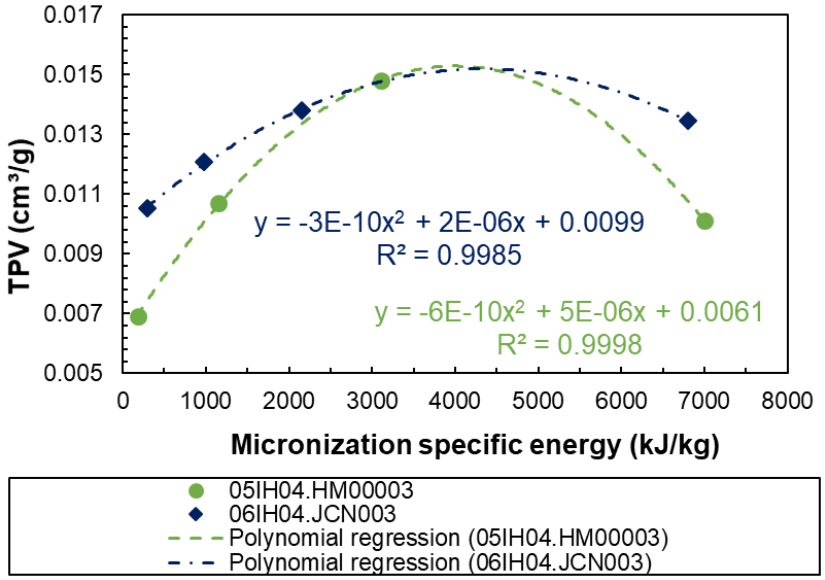

Figure 3.22: TPV as a function of Esp of the micronized materials from the SRMs 05IH04.HM00003 and 06IH04.JCN003.

Density

As shown in Figure 3.23, while for the materials obtained from the SRM 05IH04.HM00003 a fitted polynomial regression moderately explained the relation between density and Esp, a fitted power regression explained well the increase of APD of the micronized materials from the SRM 06IH04.JCN003 with the increase of Esp. These opposite behaviors observed suggested that the variation on the particle size of the SRMs did not influence the density of the micronized materials.

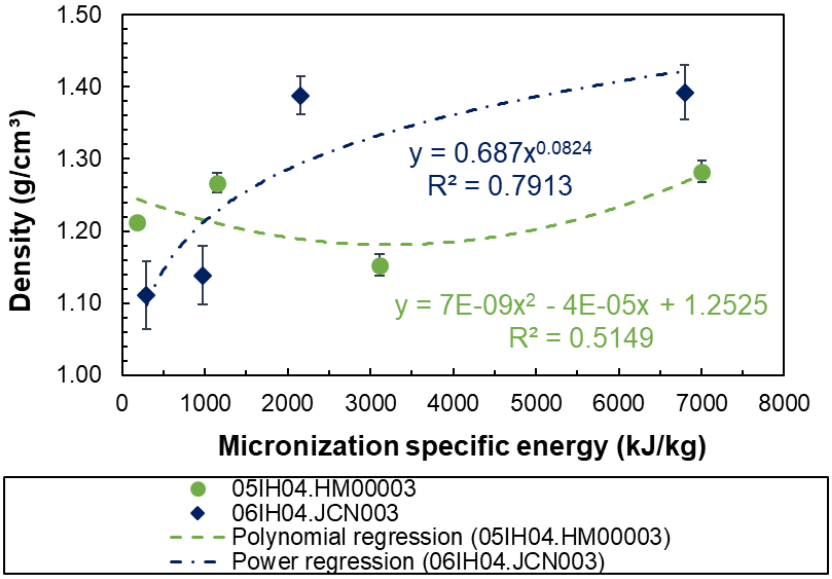

Figure 3.23: Density as a function of Esp of the micronized materials obtained from the SRMs 05IH04.HM00003 and 06IH04.JCN003.

3.3 Statistical model

SRM characteristics such as particle size and density were reported as potentially critical parameters for the quality attributes of final products [21]. Therefore, the prediction of the obtained micronized material characteristics as a function of the SRM characteristics and others that could affect the final product performance is crucial. Also, as observed on the previous sub-chapters, the micronization process parameters have a huge impact on the physical characteristics of the micronized materials.

The main objective of the implementation of a statistical model in this study was to evaluate the prediction of the micronized material characteristics as a function of the SRM characteristics and/or of the micronization process parameters.

In order to reach a final fitted model, several statistical analyses were performed considering the following:

1. Each statistical analysis was evaluated by the goodness of fit (R^2), that indicated the correlation between the X and Y variables and its predictive ability (Q^2).
2. The methodology done for all the analyses consisted on first adding all the variables and fit the data. Afterwards, if there was no statistical significance (coefficients variability surpasses the base line or if the variable importance in projection (VIP) has values below 0.5) that variable was eliminated.
3. The process (2) was repeated until reaching an acceptable model ($R^2 > 0.7$; $Q^2 > 0.5$)

Statistical analysis considering the results obtained with three starting raw material

The first statistical analysis was performed considering as X-variables the micronization process parameters (grinding pressure and feed rate) as well as the characterization of the different SRMs presented on sub-chapter 3.1. As Y-variables, it was considered the micronized material characteristics obtained from each SRM presented on sub-chapter 3.2.

The summary of the fit performed for the first statistical analysis is presented in Figure B.1 in Appendix B; the best fitting of the data was modelled by using two principal components. The respective R^2 and Q^2 values were also referred for the first ($R^2 = 0.35$; $Q^2 = -0.02$) and the second ($R^2 = 0.66$; $Q^2 = 0.34$) principal components. As observed, the difference between the R^2 and Q^2 values for each component was greater than 0.3, which may lead to an inappropriate model, as referred by Ciriani [50].

The coefficients overview and VIP plots are presented in Figure B.2 in Appendix B. The coefficients overview plot displayed the Y-variables and the corresponding X-variable coefficients. The size of the

bars is a representation of the variation of the Y-variables when the respective X-variable varies from 0 to 1; to make them comparable and for a better analysis of the results, the coefficients were normalized. The error bars indicated a confidence interval (CI) of 95% and were used to evaluate the statistical significance of the coefficients.

Since all the coefficients included the number zero, these results suggested that none of the X-variables were statistically significant for the model, when all the characteristics of the SRMs and the micronization process parameters (grinding pressure and feed rate) were considered. However, and despite being non-statistically significant, it was observed that the size of the bars for the grinding pressure and the feed rate were larger when compared with the bars of the characteristics of the SRMs, which suggested that the variation of the micronization process parameters had more influence than the variation of the SRMs characteristics.

The VIP plot summarized the overall importance of the X-variables for the Y-variables in the model. Variables with VIP values larger than 1 are important variables for the model, and variables with VIP values below 0.5 are unimportant variables. The importance of variables with values between 0.5 and 1 depends on the size of the data set used in the model.

Although being non-statistically significant, as observed in the results of the coefficients overview plot, none of the variables presented values below 0.5. It is known that opposite results between the coefficient overview and the VIP plot can be obtained in extreme cases [49], where the VIP values may lead to misleading results. Therefore, only the results observed for the coefficient overview plot were considered for this first statistical analysis.

As the SRM characteristics were not statistically significant, the X-variables and Y-variables regarding 06IH04.JCN003 were not considered for the further procedure of the statistical analysis.

Statistical analysis considering the results obtained with the starting raw material 05IH04.HM00003

The statistical analysis was performed by considering as X-variables the attributes of the SRM 05IH04.HM00003 and the JM process parameters, grinding pressure and feed rate; and considering the micronized material characteristics as the Y-variables. The software suggested two principal components to fit the data, as observed in the summary of the fit presented in Figure B.3 in Appendix B. Since the cumulative Q^2 value was above 0.5, it was considered a valid model [51].

The analysis of the coefficient overview and VIP plots was performed, and the results are shown in Figure B.4 in Appendix B. It was observed that the grinding pressure was statistically significant as the error bars of its coefficients, except for density, did not include number zero. The VIP value, which was higher than 1, also supported its importance as X-variable. However, the feed rate appeared as statistically non-significant as all the coefficient error bars included number zero, having also a low VIP value of 0.53. These results suggested that the grinding pressure had more influence than the feed rate on the characteristics of the micronized materials, which was observed for characteristics such as Dv90 and Dv50 in the results presented in sub-chapter 3.1, regarding the individual influence of the grinding process parameters on the characteristics of the micronized materials. Since, as mentioned in literature, both grinding process parameters generally had a crucial impact on the characteristics of the final micronized materials, they were considered for the remaining statistical analyses until a final fitted model was obtained.

The results obtained from the coefficients overview plot also indicated that the grinding pressure is proportional to the TPV and SSA, and inversely proportional to the PSD, APD and CS. Although not as significant as the grinding pressure, the feed rate was observed to be proportional to the PSD and the CS and inversely proportional to the TPV and SSA. The feed rate did not have a significant influence on the APD.

The grinding pressure and the feed rate were non-statistically significant for the density; that is, the variation of these process parameters did not have an influence on this Y-variable. These results were expected considering also the results obtained on sub-chapter 3.1. Therefore, this variable was excluded.

Further statistical analyses allowed the exclusive of other less important variables (Dv10, TPV and CS), and a final statistical analysis was reached; the best values of R^2 and Q^2 obtained were of $R^2 = 0.82$ and $Q^2 = 0.77$. As shown in Figure 3.24, the data was well modelled by only one principal component. In the X/Y overview also presented in Figure 3.24, it was observed that all the Y-variables were well explained by the model, as their respective Q^2 values, that were presented later on this sub-

chapter, were higher than 0.5. These results are in accordance with the previous characterization on sub-chapter 3.1. Dv90 was the most influenced Y-variable by the grinding pressure and feed rate, whereas SSA and APD presented a weaker relation with the grinding process parameters when compared with Dv90, Dv50, and span.

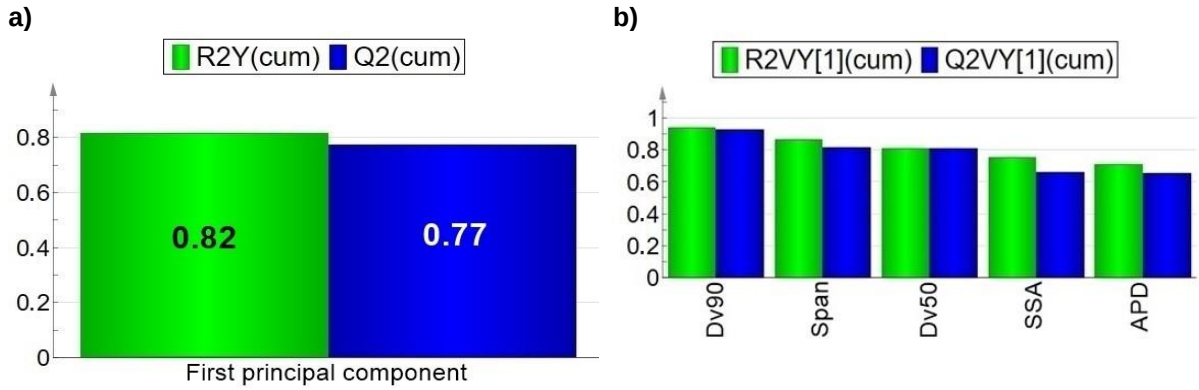

Figure 3.24: a) Summary of fit of the components and b) X/Y overview plots for the final statistical analysis.

The coefficients overview and VIP plots are represented in Figure 3.25. It can be observed that both grinding process parameters, grinding pressure and feed rate, remained statistically and non-statistically significant, respectively. The values of the coefficient overview plot are presented in Table B.1 in Appendix B. These results also suggested that the grinding pressure was proportional to SSA, and inversely proportional to Dv90, Dv50, span, and APD. Regarding the feed rate, it can be observed this variable was proportional to Dv90, Dv50, span and APD, and inversely proportional to SSA.

From the VIP plot it can again be observed that the grinding pressure was important while the feed rate was not.

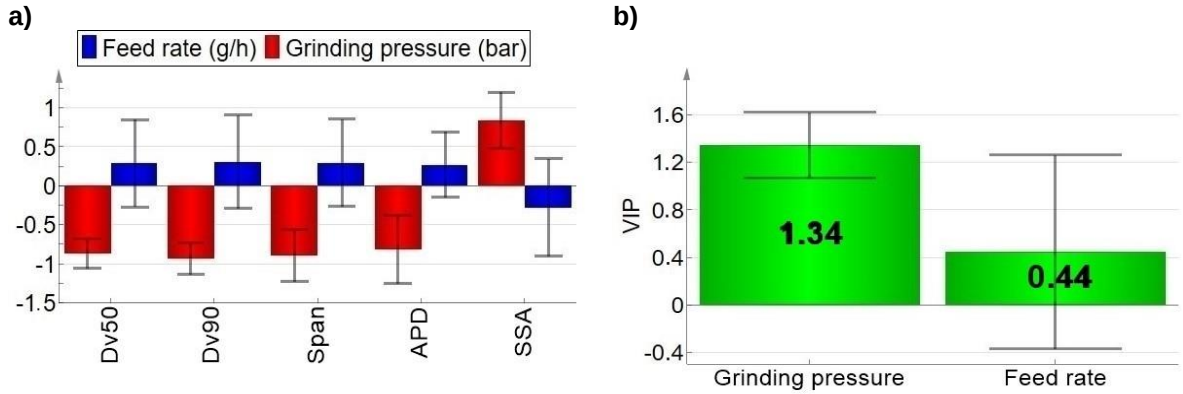

Figure 3.25: a) Coefficients overview and b) VIP plots of the X-variables and Y-variables for the fifth statistical analysis.

As the least important X-variables and Y-variables were excluded, a subsequent analysis of the observations was performed using the scores plot shown in Figure 3.26. The scores plot displayed the observations that allowed the detection, identification, and analysis of patterns, groups and possible outliers [51], were outliers corresponded to observations that were distant from the population of observations.

The observations were grouped by means of grinding pressure, that allowed the identification of the groups that correspond to the materials micronized at grinding pressures of 2 bar, 4 bar, 5.5 bar, and 6.5 bar. Considering a CI of 95%, no observations were observed outside the 2 SD limit. However, there were observations that situated far from their respective grinding pressure group and were considered possible outliers. These observations were JCN005, JCN007, JCN008, and JCN018.

To conclude whether to include or exclude these observations from the model, the DModX plot also presented in Figure 3.26 was analysed. The DModX plot, displayed in normalized units, is the distance of each observation to the X model plane, being proportional to the residual SD of each X-observation [51]. As can be observed, all the observations, and in particular those that deviated from each group, had a distance below the critical DModX value; therefore, all the observations were considered for the model and no outliers were detected.

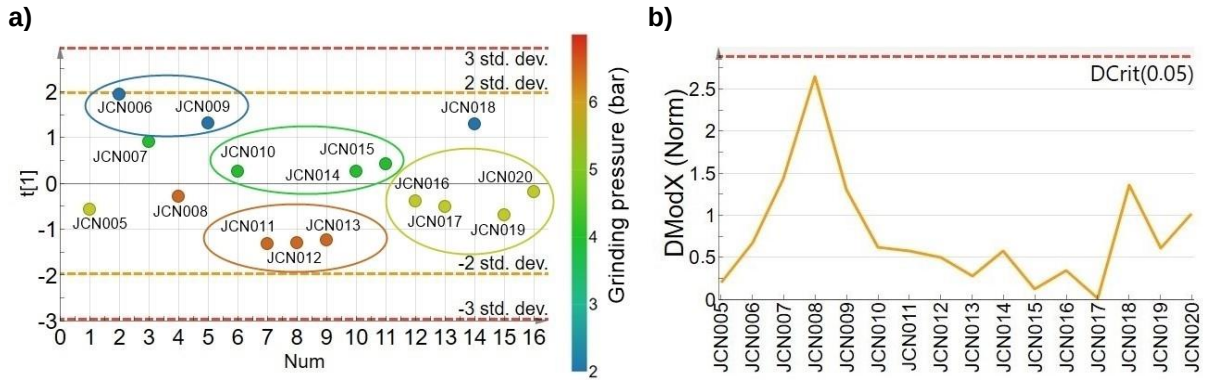

Figure 3.26: a) Scores plot displaying the observations by means of constant grinding pressure, and b) DmodX plot for all the observations considered in the fifth statistical analysis.

The loadings plot, presented in Figure 3.27, gave an important information about the correlation between variables and how strongly the principal component explained each variable. As observed, the grinding pressure and all the Y-variables were well explained by the first principal component as these variables had values near -1 and 1. However, the feed rate was poorly explained as it was close to the origin. To analyse the correlation between variables, a line was vertically traced from a selected Y-variable (Dv90) and the remaining X and Y-variables were projected into it. Variables that lied near to each other were positively correlated, while opposite variables were negatively correlated [61]. All the Y-variables, except for SSA, were inversely proportional to the grinding pressure and proportional to the feed rate; opposite results were obtained for the SSA. These results supported the previously obtained results for the coefficients overview plot.

A strong relationship between the X-variables and Y-variables was also observed using the Inner relation plot, also shown in Figure 3.27. The inner relation plot presented the relation between the summarized X-variables and Y-variables (t1 and u1, respectively) [61]. As only a small scatter was verified around the diagonal line, having a R^2 of 0.95, a strong relation between the X-variables and Y-variables was verified.

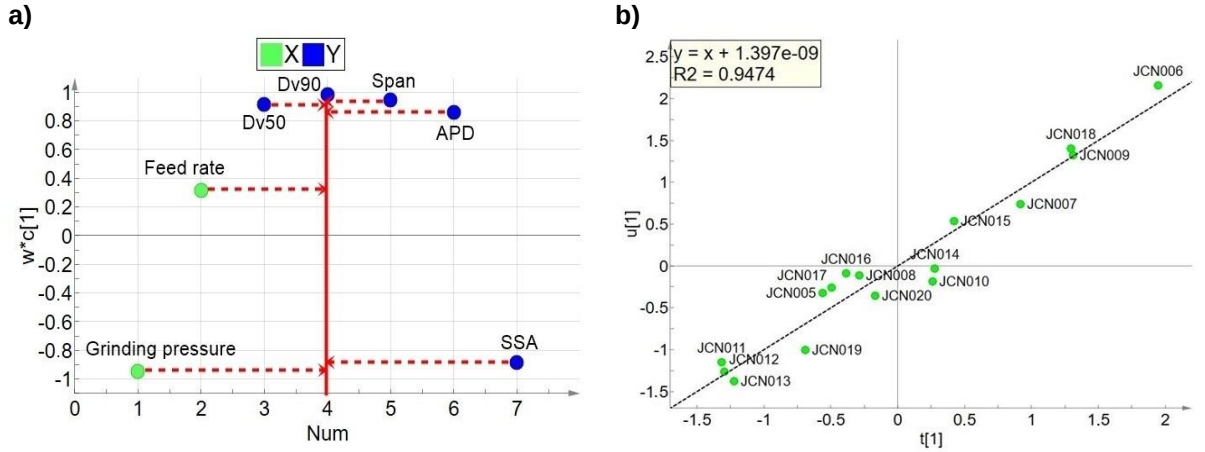

Figure 3.27: a) Loadings plot with the traced line projected from Dv90, and b) Inner relation plot for the fifth statistical analysis.

A further analysis was performed using the Biplot presented in Figure 3.28. A scaling factor was used to display the data of both scores and loadings plot, which allowed the interpretation of the observations

in terms of variables [61, 62]. As an example, for the interpretation of this plot, the micronized material 06IH04M.JCN006 (observation JCN006) presented the lowest SSA and the highest Dv90 of the micronized materials from the SRM 05IH04.HM00003. Therefore, and as observed in the Biplot, this observation was situated near the Dv90 variable, and far from the SSA variable. This observation also presented a strong positive and negative correlation with Dv90 and SSA, respectively. The observed results in this plot were in accordance with the previously obtained results on subchapter 3.1.

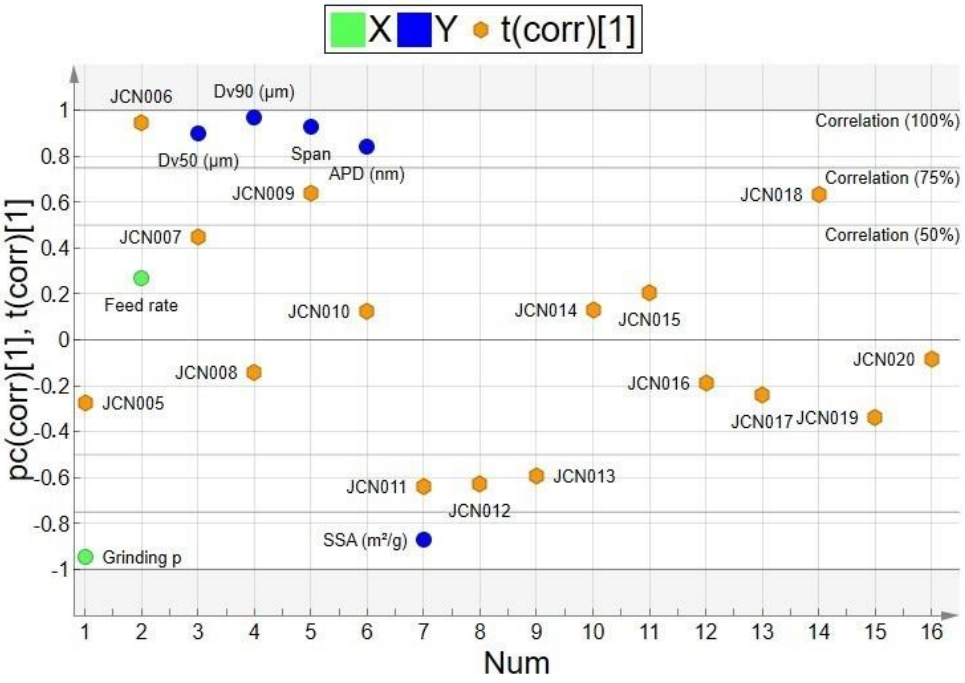

Figure 3.28: Biplot displaying the observations and variables considered for the fifth statistical analysis.

Predictions

The Observed vs Predicted plots were used to evaluate the model predictions, by ploting the observed and the predicted Y-variable. For each Y-variable, the observed and predicted plots are presented in Figure B.5 in Appendix B. As can be observed, the R^2, Q^2 and RMSEcv values were displayed for each Y-variable. By analysing the R^2, it was concluded that all the Y-variables were well modelled, presenting an $R^2 > 0.7$. Observations that fell far from the regression line were considered possible outliers and were studied; as an example, in the plot corresponding to the span variable, observation JCN014 was considered a possible outlier. However, since this observation fitted well for other Y-variables, it was not excluded.

The observed Q^2 values for all the Y-variables were good as they were higher than 0.5. Therefore, the Y-variables were well predicted by the model. The RMSEcv is a measure of the predictive power of the model, and its magnitude depends on the magnitude of each Y-variable. Except for the SSA, it was observed that the RMSEcv values regarding each Y-variable were relatively small. The considerable RMSEcv value for SSA may be explained by the high equipment error of measurement (2.40 m²/g).

A further analysis using contour plots was performed to analyse how the X-variables influenced the Y-variables. The contour plots presented in Figure B.6 in Appendix B displayed the obtained values for each Y-variable with the variation of the X-variables. The same results regarding the relation between the X-variables and Y-variables of the coefficients overview plot presented before were observed. Higher grinding pressures and lower feed rates led to lower SSA values, and to higher Dv90, span, Dv50 and APD values.

Analysing the contour plot of Dv90, it was observed that lower particles sizes could be obtained at higher grinding pressure and lower feed rate conditions. Lower grinding pressure and higher feed rate conditions could also be performed to obtain larger particles sizes.

As reported in literature [11, 64], the particle size of the materials is crucial for inhalation, and should be smaller than 5 µm for formulations for inhalation. All 16 micronizations performed for the SRM 05IH04.HM00003 presented a particle size lower or similar than 5 µm. Only a small region at lower grinding pressures and higher feed rates presented a particle size larger than 5 µm. Therefore, this region should be avoided when micronized materials suitable for inhalation are desired.

For span, micronization conditions using higher grinding pressures and lower feed rates may be used to obtain micronized materials with a more homogeneous PSD. Regarding SSA, higher SSA values for the micronized materials of the SRM 05IH04.HM00003 were obtained by increasing the grinding pressure and decreasing the feed rate, as observed in the SSA contour plot. However, in sub-chapter 3.1 a maximum SSA value was observed in an Esp value between the fragmentation and attrition regimes. Micronized materials with lower particle size (higher SSA) are preferred for inhalation since it increases the solubility of the API [64]. Therefore, micronizations using intermediate Esp values may also be preferred. Regarding the APD, lower values would also be obtained for higher grinding pressures and lower feed rates.

Therefore, micronizations performed at the fragmentation regime are preferred, as the micronized materials could be more stable than materials micronized in the attrition regime due to the amorphous regions that could exist on the particles [21].

4 Conclusions and future perspectives

4.1 Conclusions

In this work, a statistical model was successfully implemented, in order to predict the physical characteristics of the micronized materials using the JM technique while varying the main micronization process parameters and for starting raw materials with different physical characteristics.

The two different SRMs, 05IH04.HM00003 and 06IH04.JCN003, with different particle size distributions were used to perform this work, where the material 06IH04.JCN003 was obtained via a manual grinding process of the SRM 05IH04.HM00003. Both SRMs presented the same plate-like morphology, polymorphic form and were mesoporous. The increase of span of the SRM 06IH04.JCN003 when compared with the SRM 05IH04.HM00003 was related to a non-uniform manual grind. The manual grinding process did not affect the crystallinity nor the polymorphic form of the SRMs. Therefore, the higher peak intensities observed for the SRM 06IH04.JCN003 when compared with the SRM 05IH04.HM00003 were associated to the variability of the measuring technique.

The SRM 05IH04.HM00003 was a hard and very elastic material, thus higher energies were required to overcome its elastic properties and reduce its particle size. Inconclusive results regarding the elasticity and hardness of the SRM 06IH04.JCN003 were obtained and were not presented. The decrease of particle size for the SRMs did not affect the SSA, APD and TPV. However, it led to an increase of density.

The materials micronized from the SRM 05IH04.HM00003 presented the same plate-like morphology, polymorphic form and were also mesoporous. The crystallinity of the micronized materials did not change with the increase of Esp, and no recrystallization was observed for a micronized sample after 1 week at room conditions (T=25ºC and a RH=50%). Dv10, Dv50 and Dv90 of the micronized materials decreased with the increase of Esp, showing a rapid decrease of particle size at lower Esp values and reaching a plateau at approximately 0.60 µm, 1.60 µm and 3.40 µm, respectively. The span decreased with the increase of Esp, meaning that the particle size distributions is more homogeneous for higher Esp. The plate-like morphology and polymorphic form of the micronized materials did not change with the increase of Esp. The weak relation found for the CS with the increase of Esp was related to the non-equilibrium between the fragmentation process and the recrystallization of small amorphous fractions of the micronized materials.

The impact of the micronization energy and correspondent regime was clearly observed. For the fragmentation regime (lower Esp values), the SSA and TPV showed a rapid increase with the increase of Esp. For higher Esp values (attrition regime), it was observed a decrease. These behavior could have possibly been due to a surface amorphization and subsequent rapid surface rearrangement during the milling process. For the APD, a poor relation was observed in the fragmentation regime, which suggested a non-uniform formation of pore sizes; whereas for the attrition regime, a plateau at approximately 9 nm was reached. No relation between density and the increase of Esp was observed.

Considering the relation of the material characteristics with the grinding pressure and feed rate individually, it was observed that both grinding process parameters did not influence the morphology, crystallinity and the polymorphic form of the micronized materials. It was not possible to stablish a relation between the CS, APD and density with the grinding process parameters, as no linear correlation was found for the different intervals of both pressure and feed rate. For the remaining micronized material characteristics (Dv10, Dv50, Dv90, span, SSA and TPV), it was observed that the grinding pressure had a higher influence on these parameters than the feed rate. The micronizations performed at the fragmentation regime are preferred, as the micronized materials could be more stable than materials micronized in the attrition regime due to the amorphous regions that could exist on the particles, as already mentioned in literature.

For the comparison of the micronized materials obtained from SRMs with different particle size, it was concluded that, except for the crystallinity, SSA and TPV, no relation between the decrease of particle size of the SRMs and the micronized material characteristics was observed. The micronized materials from the SRM 06IH04.JCN003 were less crystalline than the micronized materials from the SRM 05IH04.HM00003. The crystallinity of the micronized materials of both SRMs did not change with the increase of Esp. For the analysis of SSA and TPV as a function of Esp, the micronized materials of both SRMs presented a similar behavior, and the micronized materials from the SRM 06IH04.JCN003

presented higher SSA and TPV values at similar Esp values than the micronized materials from the SRM 05IH04.HM00003.

To implement the statistical model, the micronization process parameters (grinding pressure and feed rate) as well as the characterization of both SRMs were considered as X-variables. The characteristics of the micronized material were considered as Y-variables, with a total of 16 observations. The characteristics of the SRM 06IH04.JCN003 and the respective micronized materials were excluded as they were non-significant for the model. Density, Dv10, TPV and CS were also excluded from the model as these variables presented lower and even negative Q^2 values, affecting negatively the predictive ability of the model.

The final fitted model presented one principal component, and the Dv90, span, Dv50, SSA and APD of the micronized materials from the SRM 05IH04.HM00003 were well modelled. A strong relation between the grinding process parameters and the micronized material characteristics was observed for the fitted model. Between grinding pressure and feed rate, grinding pressure influenced more the micronized material characteristics than the feed rate, which was observed and was supported by the results presented in subchapter 3.1. The Dv90 was the most predictive variable with a Q^2 of 0.93, while APD was the least predictive with a Q^2 of 0.65.

Considering the contour plots, micronization conditions with higher grinding pressures and lower feed rates led to lower particle size, APD and more homogeneous PSD. Opposite results may be obtained by using micronization conditions with lower grinding pressure and higher feed rates. For SSA, however, a maximum value was observed at an intermediate Esp value (intermediate grinding pressures and feed rates).

All the micronization conditions performed for the SRM 05IH04.HM00003 are suitable to obtain particles for inhalation, as they presented a particle size lower or similar than 5 µm. Considering the Dv90 contour plot, only a small region at lower grinding pressures and higher feed rates presented a particle size larger than 5 µm. Therefore, this region should be avoided when micronizing materials suitable for inhalation. To obtain particles with higher SSA values, micronizations using intermediate Esp values (between the fragmentation and attrition regimes) may also be preferred.

4.2 Future Perspectives

Performing more micronization tests with a constant grinding pressure or a constant feed rate in order to study the micronized material characteristics (as studied for materials micronized with similar Esp values) may be interesting.

Since nanoindentation by AFM was not the most suitable technique to measure hardness and elastic properties of these materials, and knowing that these characteristics are considered crucial parameters that could affect the micronization behaviour, it would be necessary to use other measuring techniques, such as nanoindentation, which is a well-known technique widely used to characterize the mechanical properties of APIs. It would be also interesting to compare the micronization behavior of this API with other APIs with different properties.

Considering only two SRMs with different particle size may be the reason why the SRM characteristics used as X-variables in the statistical model appeared as not statistically significant. Thus, further studies using more SRMs with different characteristics are necessary. More micronized samples for each SRM are also necessary for a better understanding of the individual influence of the grinding process parameters grinding pressure and feed rate.

Adding more material characteristics that may be important for other pharmaceutical fields (such as hygroscopicity and surface energy). and other micronization process parameters and observations, may help to implement a more complex model. Using different APIs to verify if their micronized material characteristics could also be predicted using this model is also very important.

References

[1] H. Kalasz and I. Antal, “Drug Excipients,” *Curr. Med. Chem.*, 2006.

[2] D. R. Hess, “Nebulizers: Principles and performance,” in *Respiratory Care*, 2000.

[3] T. V Thulasiramaraju, B. T. Kumar, and M. Nikilesh Babu, “Pulmonary Drug Delivery System: an Overview,” *Asian J. Res. Pharm. Sci. Biotechnol.*, vol. 1, no. 1, pp. 16–34, 2013.

[4] J. L. Rau, “The inhalation of drugs: Advantages and problems,” *Respir. Care*, 2005.

[5] D. Price and H. Chrystyn, “Concept review of dry powder inhalers: Correct interpretation of published data,” *Multidiscip. Respir. Med.*, 2015.

[6] R. O. Williams and C. Hu, “Moisture uptake and its influence on pressurized metered-dose inhalers,” *Pharm. Dev. Technol.*, vol. 5, no. 2, pp. 153–162, 2000.

[7] J. S. Patil and S. Sarasija, “Pulmonary drug delivery strategies: A concise, systematic review,” *Lung India*. 2012.

[8] Y. Zhang, H. F. Chan, and K. W. Leong, “Advanced materials and processing for drug delivery: The past and the future,” *Advanced Drug Delivery Reviews*. 2013.

[9] Z. Sun, N. Ya, R. C. Adams, and F. S. Fang, “Particle size specifications for solid oral dosage forms: A regulatory perspective,” *American Pharmaceutical Review*, vol. 13, no. 4. pp. 68–73, 2010.

[10] Y. Qiu, Y. Chen, G. Zhang, L. Liu, and W. Porter, *Developing Solid Oral Dosage Forms*. 2009.

[11] S. Jabbal, G. Poli, and B. Lipworth, “Does size really matter?: Relationship of particle size to lung deposition and exhaled fraction,” *J. Allergy Clin. Immunol.*, vol. 139, no. 6, pp. 2013-2014.e1, 2017.

[12] K. Stank and H. Steckel, “Physico-chemical characterisation of surface modified particles for inhalation,” *Int. J. Pharm.*, vol. 448, no. 1, pp. 9–18, 2013.

[13] C. Moura, F. Neves, and E. Costa, “Impact of jet-milling and wet-polishing size reduction technologies on inhalation API particle properties,” *Powder Technol.*, vol. 298, pp. 90–98, 2016.

[14] Z. H. Loh, A. K. Samanta, and P. W. Sia Heng, “Overview of milling techniques for improving the solubility of poorly water-soluble drugs,” *Asian J. Pharm. Sci.*, vol. 10, no. 4, pp. 255–274, 2014.

[15] T. Peng *et al.*, “Influence of physical properties of carrier on the performance of dry powder inhalers,” *Acta Pharm. Sin. B*, vol. 6, no. 4, pp. 308–318, 2016.

[16] C. Kumaresan, N. Subramanian, M. Gover Antoniraj, and K. Ruckmani, “Dry powder inhaler - Formulation aspects,” *Pharma Times*, vol. 44, no. 10, pp. 14–18, 2012.

[17] L. Maggi, R. Bruni, and U. Conte, “Influence of the moisture on the performance of a new dry powder inhaler,” *Int. J. Pharm.*, 1999.

[18] H. K. Chan, “What is the role of particle morphology in pharmaceutical powder aerosols?,” *Expert Opin. Drug Deliv.*, vol. 5, no. 8, pp. 909–914, 2008.

[19] H. G. Brittain, S. R. Byrn, and E. Lee, *Structural aspects of polymorphism*, vol. 192. 2016.

[20] N. Rasenack and B. W. Müller, “Micron-Size Drug Particles: Common and Novel Micronization Techniques,” *Pharm. Dev. Technol.*, vol. 9, no. 1, pp. 1–13, 2004.

[21] M. Nakach, J. R. Authelin, C. Corsini, and G. Gianola, “Jet milling industrialization of sticky active pharmaceutical ingredient using quality-by-design approach,” *Pharm. Dev. Technol.*, vol. 24, no. 7, pp. 849–863, 2019.

[22] V. Joshi, S. Dwivedi, and G. H. Ward, “Increase in the specific surface area of budesonide during storage postmicronization,” *Pharm. Res.*, vol. 19, no. 1, pp. 7–12, 2002.

[23] N. Midoux, P. Hošek, L. Pailleres, and J. R. Authelin, “Micronization of pharmaceutical substances in a spiral jet mill,” *Powder Technol.*, vol. 104, no. 2, pp. 113–120, 1999.

[24] M. Nakach, J. R. Authelin, A. Chamayou, and J. Dodds, “Comparison of various milling technologies for grinding pharmaceutical powders,” *Int. J. Miner. Process.*, vol. 74, no. SUPPL., 2004.

[25] A. Chamayou and J. A. Dodds, “Chapter 8 Air Jet Milling,” *Handb. Powder Technol.*, vol. 12, no. 33, pp. 421–435, 2007.

[26] F. Muller, R. Polke, and G. Schadel, “Spiral jet mills: hold up and scale up,” *Int. J. Miner. Process.*, vol. 44–45, pp. 315–326, 1996.

[27] I. Meccanica, “Tecnologia Meccanica II,” pp. 1–23, 2008.

[28] A. Nayeri, “Spiral Jet Mill,” *Ceramic Industry*, 2009.

[29] R. MacDonald, D. Rowe, E. Martin, and L. Gorringe, “The spiral jet mill cut size equation,” *Powder Technol.*, vol. 299, pp. 26–40, 2016.

[30] Q. Zhang, J. Kano, and F. Saito, “Chapter 11 Fine Grinding of Materials in Dry Systems and Mechanochemistry,” *Handb. Powder Technol.*, vol. 12, no. 07, pp. 509–528, 2007.

[31] V. Chikhalia, R. T. Forbes, R. A. Storey, and M. Ticehurst, “The effect of crystal morphology and mill type on milling induced crystal disorder,” *Eur. J. Pharm. Sci.*, vol. 27, no. 1, pp. 19–26, 2006.

[32] P. K. Deb, S. N. Abed, A. M. Y. Jaber, and R. K. Tekade, *Particulate Level Properties and its Implications on Product Performance and Processing*. Elsevier Inc., 2018.

[33] R. Patel, A. Baria, and N. Patel, “An overview of size reduction technologies in the field of pharmaceutical manufacturing,” *Asian J. Pharm.*, vol. 2, no. 4, p. 216, 2008.

[34] I. Y. Saleem and H. D. C. Smyth, “Micronization of a soft material: Air-jet and micro-ball milling,” *AAPS PharmSciTech*, vol. 11, no. 4, pp. 1642–1649, 2010.

[35] S. Zügner, K. Marquardt, and I. Zimmermann, “Influence of nanomechanical crystal properties on the comminution process of particulate solids in spiral jet mills,” *Eur. J. Pharm. Biopharm.*, vol. 62, no. 2, pp. 194–201, 2006.

[36] “Use of Co-milling to improve physical stability of amorphous salbutamol sulphate,” *AIChE Annu. Meet. Conf. Proc.*, no. Figure 1, pp. 4–7, 2008.

[37] F. M., S. S., and P. J.F., “Sizing and morphology analysis of milled olanzapine, paroxetine and gabapentin particles using hot stage microscopy and laser diffractometry,” *Ann. Med.*, vol. 50, no. Supplement 1, pp. S54–S55, 2018.

[38] A. W. Newman and S. R. Byrn, “Solid-state analysis of the active pharmaceutical ingredient in drug products,” *Drug Discov. Today*, vol. 8, no. 19, pp. 898–905, 2003.

[39] E. A. De Moura *et al.*, “Solid-state form characterization of riparin i,” *Molecules*, vol. 22, no. 10, pp. 1–13, 2017.

[40] M. Descamps and J. F. Willart, “Perspectives on the amorphisation/milling relationship in pharmaceutical materials,” *Adv. Drug Deliv. Rev.*, vol. 100, pp. 51–66, 2016.

[41] N. Stieger and W. Liebenberg, “Recrystallization of Active Pharmaceutical Ingredients,” in *Crystallization - Science and Technology*, 2012.

[42] S. Sud and A. Kamath, “Methods of Size Reduction and Factors Affecting Size Reduction in Pharmaceutics,” *Int. Res. J. Pharm.*, vol. 4, no. 8, pp. 57–64, 2013.

[43] N. V. Rama Rao and G. C. Hadjipanayis, “Influence of jet milling process parameters on particle size, phase formation and magnetic properties of MnBi alloy,” *J. Alloys Compd.*, vol. 629, pp. 80–83, 2015.

[44] A. Original, “Desenvolvimento De Um Modelo Experimental De,” vol. 20, no. 3, pp. 2011–2013, 2012.

[45] G. Shmueli, “To explain or to predict?,” *Stat. Sci.*, vol. 25, no. 3, pp. 289–310, 2010.

[46] S. Maitra and J. Yan, “<PCA vs PCL dimension reduction.pdf>,” pp. 79–90, 2008.

[47] S. Getting, “What is Multivariate Analysis What is a Projection ? Reduction of dimensionality , model in latent variables,” vol. 1, no. 29.

[48] R. Todeschini, “Useful and unuseful summaries of regression models,” *Group*, pp. 1–9.

[49] M. Analysis and F. A. Questions, “SIMCA-P F.a.q.,” pp. 1–9.

[50] M. C. Rodrigues, “SYNTHESIS OF QUATERNARY AMMONIUM SALTS USING BATCH AND CONTINUOUS TECHNOLOGIES Examination Committee :,” no. July, 2017.

[51] L. Eriksson, T. Byrne, E. Johansson, J. Trygg, and C. Vikström, “Process Analytical Technology (PAT) and Quality by Design (QbD),” *Multi- Megavariate Data Anal. Value From Data*, pp. 323–355, 2013.

[52] S. Chen, A. Y. Sheikh, and R. Ho, “Evaluation of effects of pharmaceutical processing on structural disorders of active pharmaceutical ingredient crystals using nanoindentation and high-resolution total scattering pair distribution function analysis,” *J. Pharm. Sci.*, vol. 103, no. 12, pp. 3879–3890, 2014.

[53] G. Liu, “Hammer milling and jet milling fundamentals,” *Chem. Eng. Prog.*, vol. 113, no. 6, 2017.

[54] D. F. Roa, P. R. Santagapita, M. P. Buera, and M. P. Tolaba, “Ball Milling of Amaranth Starch-Enriched Fraction. Changes on Particle Size, Starch Crystallinity, and Functionality as a Function of Milling Energy,” *Food Bioprocess Technol.*, vol. 7, no. 9, pp. 2723–2731, 2014.

[55] H. Adi, D. Traini, H. K. Chan, and P. M. Young, “The influence of drug morphology on the aerosolisation efficiency of dry powder inhaler formulations,” *J. Pharm. Sci.*, 2008.

[56] K. Raza, “Polymorphism: The Phenomenon Affecting the Performance of Drugs,” *SOJ Pharm. Pharm. Sci.*, 2014.

[57] Y. Sugamura *et al.*, “Effect of particle size of drug on conversion of crystals to an amorphous state in a solid dispersion with crospovidone,” *Chem. Pharm. Bull.*, vol. 59, no. 2, pp. 235–238, 2011.

[58] N. Dujardin, J. F. Willart, E. Dudognon, F. Danède, and M. Descamps, “Mechanism of solid state amorphization of glucose upon milling,” *J. Phys. Chem. B*, vol. 117, no. 5, pp. 1437–1443, 2013.

[59] M. Suśniak, P. Pałka, and J. Karwan-Baczewska, “Influence of milling time on the crystallite size of AlSi5Cu2/SiC composite powder,” *Arch. Metall. Mater.*, vol. 61, no. 2B, pp. 977–980, 2016.

[60] M. Toozandehjani, K. A. Matori, F. Ostovan, S. A. Aziz, and M. S. Mamat, “Effect of milling time on the microstructure, physical and mechanical properties of Al-Al2O3 nanocomposite synthesized by ball milling and powder metallurgy,” *Materials (Basel).*, vol. 10, no. 11, 2017.

[61] MKS Umetrics, “User Guide to SIMCA - Version 13,” pp. 1–621, 2012.

[62] Vinzi, *Handbook of Statistical Bioinformatics*. 2011.

[63] Y.-W. Lin, J. Wong, L. Qu, H.-K. Chan, and Q. Zhou, “Powder Production and Particle Engineering for Dry Powder Inhaler Formulations,” *Curr. Pharm. Des.*, vol. 21, no. 27, pp. 3902–3916, 2015.

[64] S. M. Snorek *et al.*, “PQRI recommendations on particle-size analysis of drug substances used in oral dosage forms,” *J. Pharm. Sci.*, 2007.

Appendix A

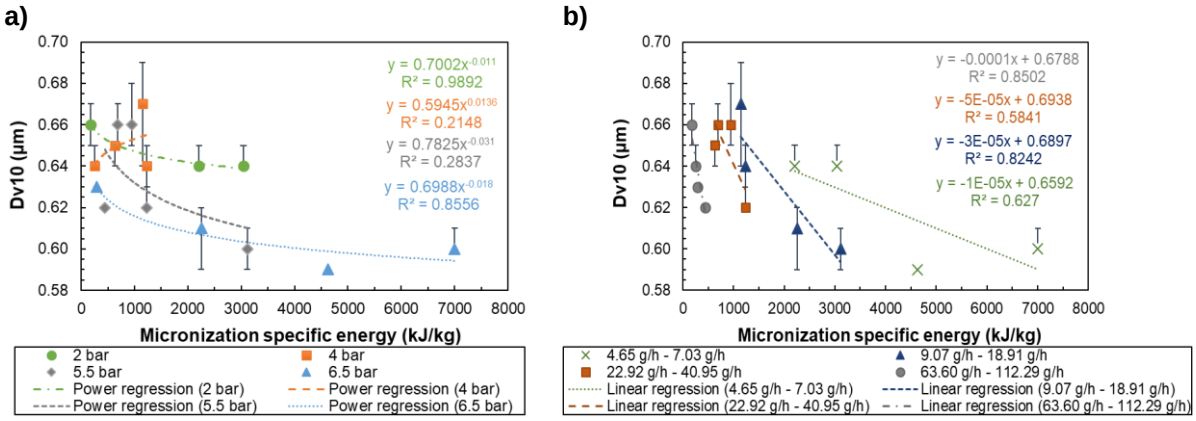

Figure A.1: Dv10 as a function of Esp of the micronized materials from the SRM 05IH04.HM00003, grouped by means of a) constant grinding pressure and b) feed rate intervals.

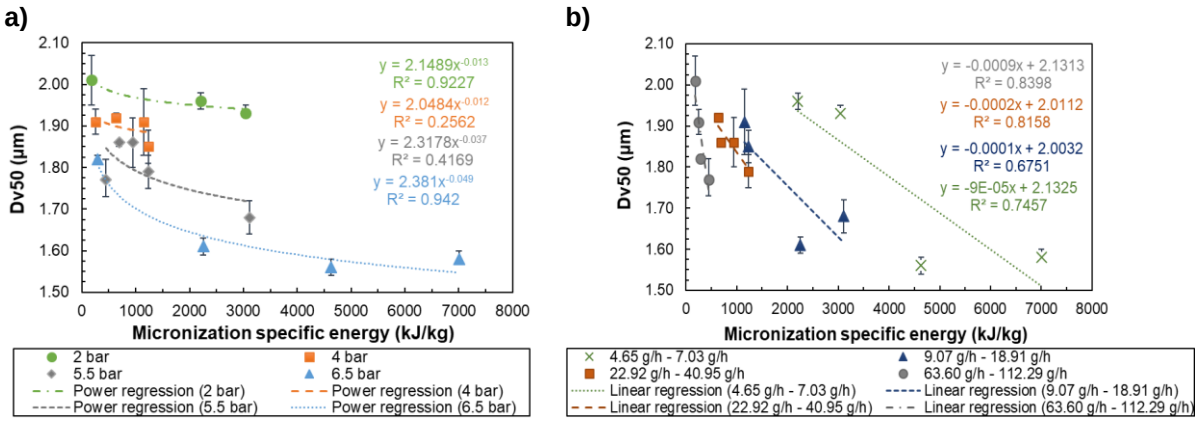

Figure A.2: Dv50 as a function of Esp of the micronized materials from the SRM 05IH04.HM00003, grouped by means of a) constant grinding pressure and b) feed rate intervals.

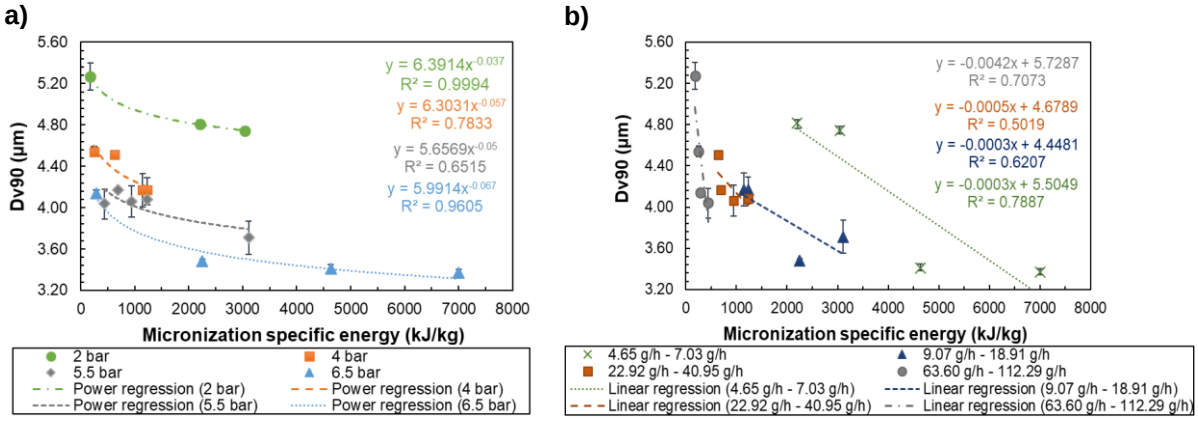

Figure A.3: Dv90 as a function of Esp of the micronized materials from the SRM 05IH04.HM00003, grouped by means of a) constant grinding pressure and b) feed rate intervals.

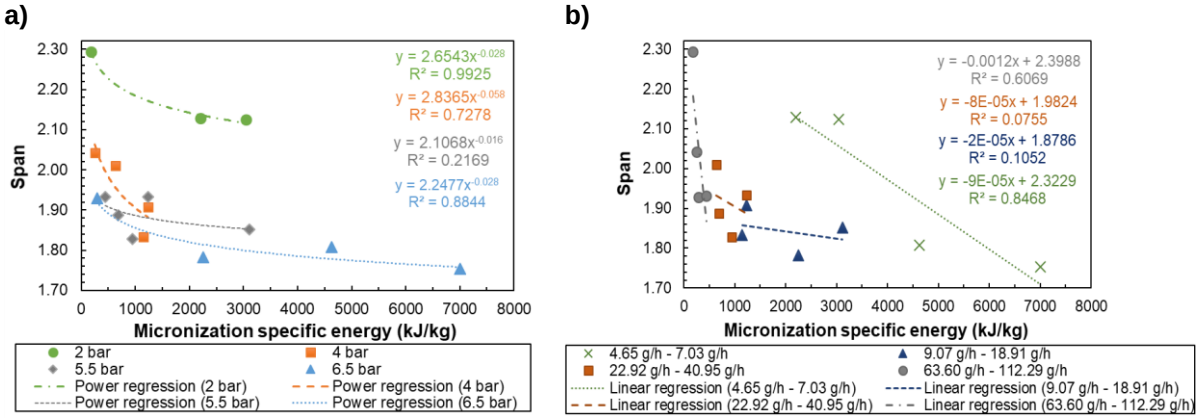

Figure A.4: Span as a function of Esp of the micronized materials from the SRM 05IH04.HM00003, grouped by means of a) constant grinding pressure and b) feed rate intervals.

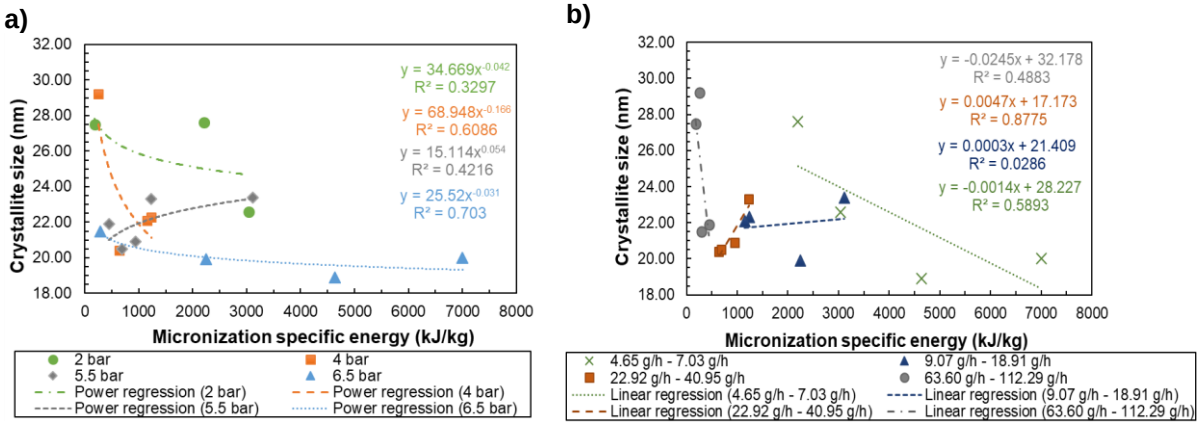

Figure A.5: CS as a function of Esp of the micronized materials from the SRM 05IH04.HM00003, grouped by means of a) constant grinding pressure and b) feed rate intervals.

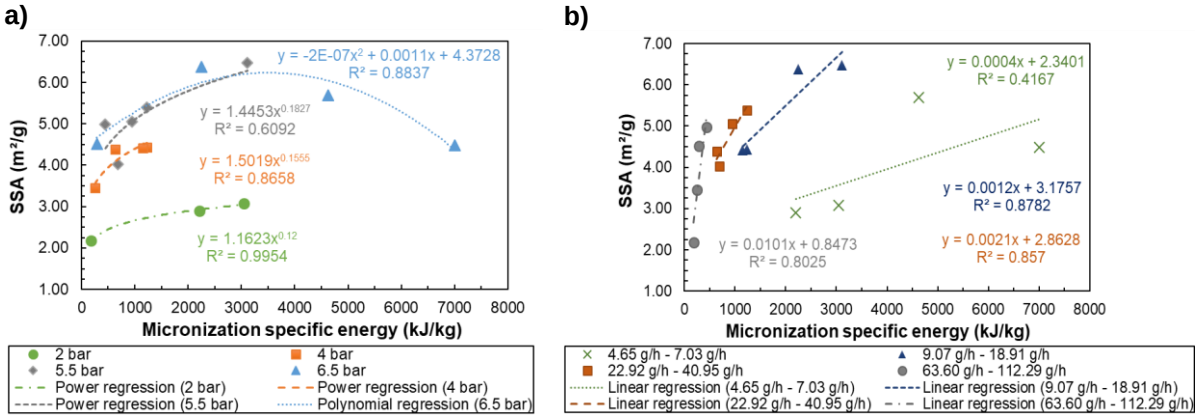

Figure A.6: SSA as a function of Esp of the micronized materials from the SRM 05IH04.HM00003, grouped by means of a) constant grinding pressure and b) feed rate intervals.

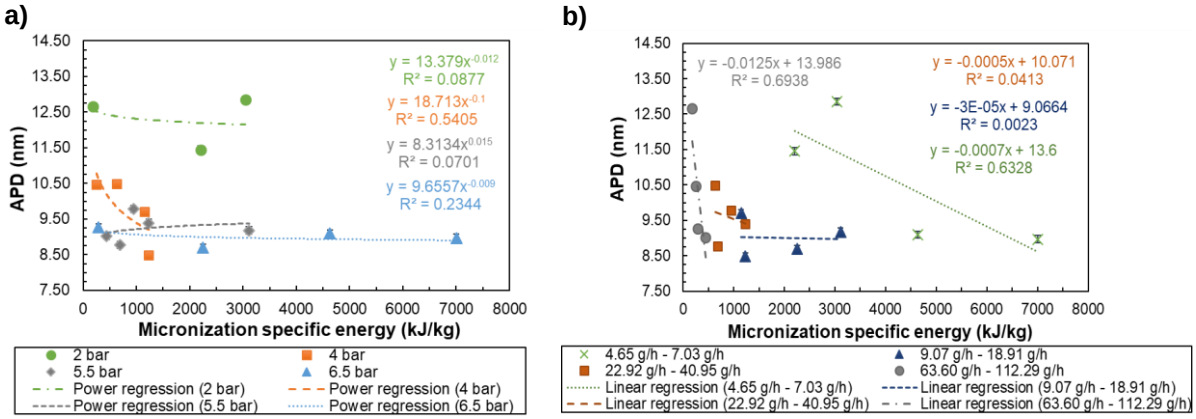

Figure A.7: APD as a function of Esp of the micronized materials from the SRM 05IH04.HM00003, grouped by means of a) constant grinding pressure and b) feed rate intervals.

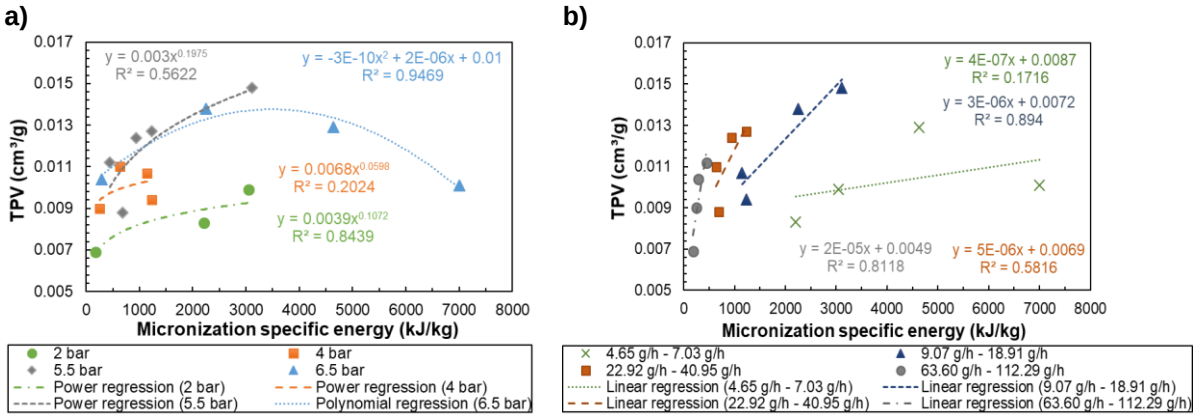

Figure A.8: TPV as a function of Esp of the micronized materials from the SRM 05IH04.HM00003, grouped by means of a) constant grinding pressure and b) feed rate intervals.

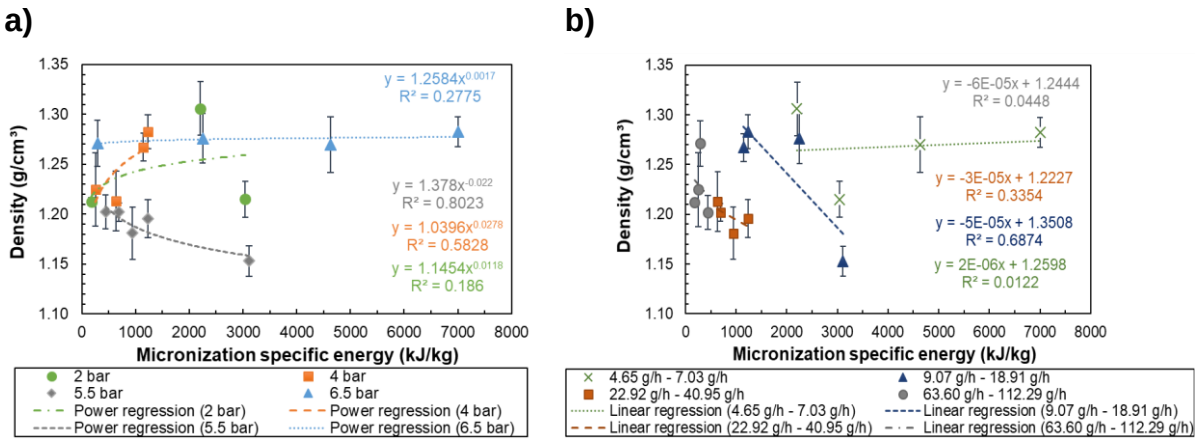

Figure A.9: Density as a function of Esp of the micronized materials from the SRM 05IH04.HM00003, grouped by means of a) constant grinding pressure and b) feed rate intervals.

Appendix B

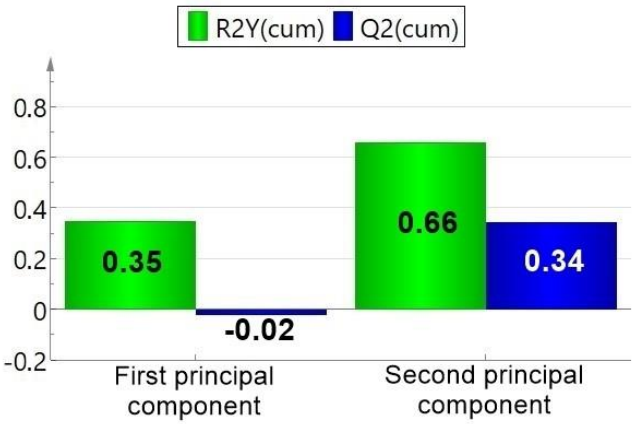

Figure B.1: Summary of fit of the components for the first statistical analysis.

a)

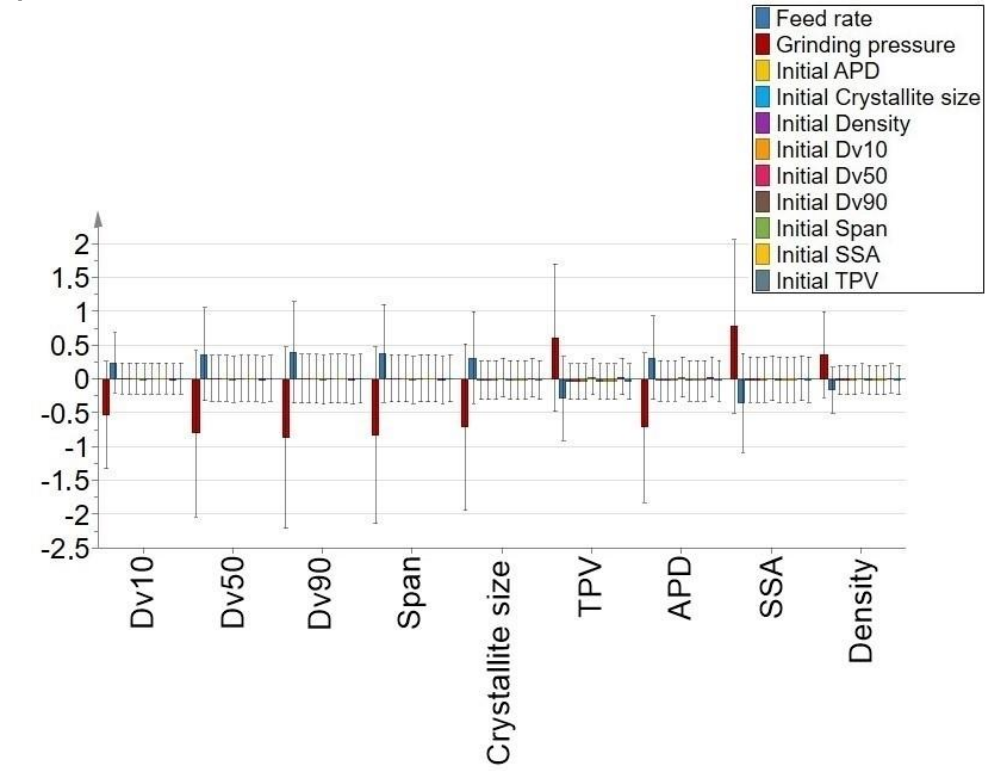

b)

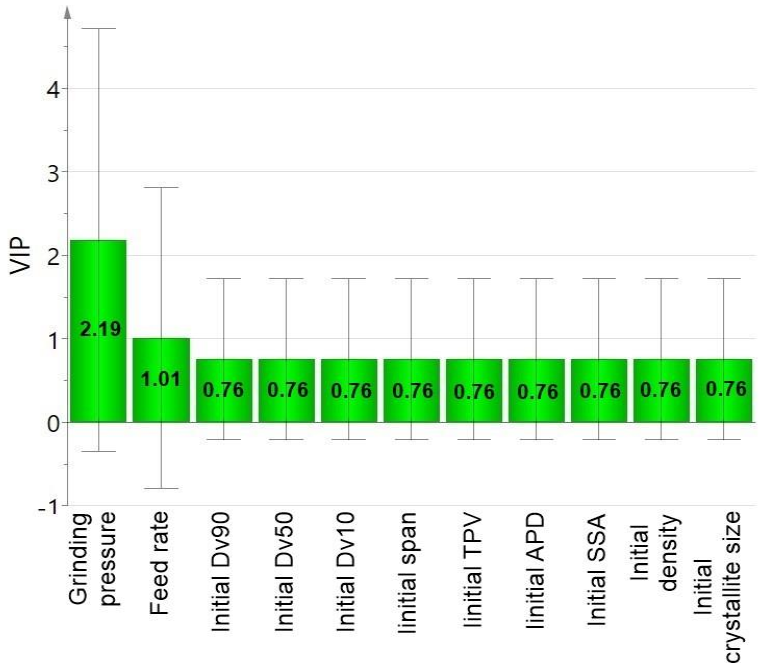

Figure B.2: a) Coefficients overview and b) VIP plots of the X-variables and Y-variables for the first statistical analysis.

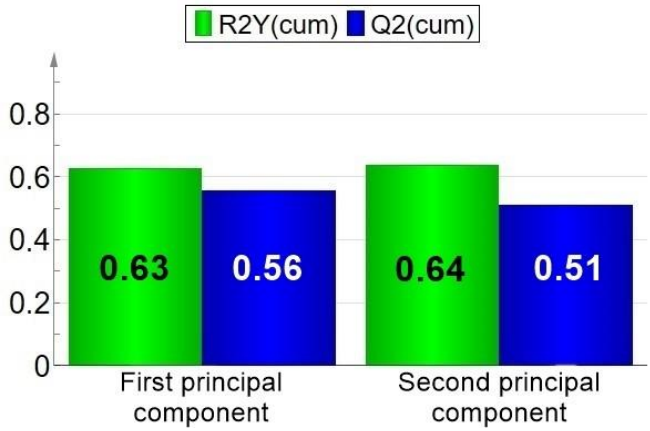

Figure B.3: Summary of fit of the components for the second statistical analysis.

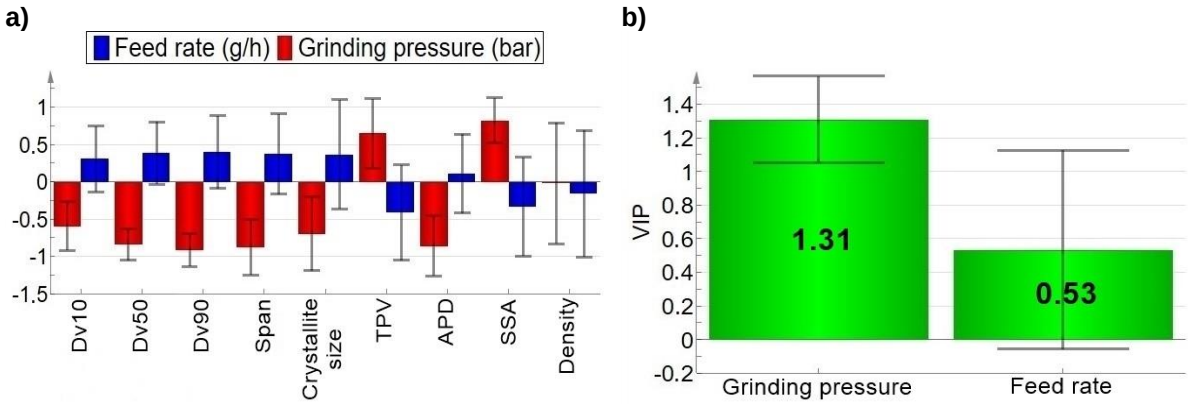

Figure B.4: a) Coefficients overview and b) VIP plots of the X-variables and Y-variables for the second statistical analysis.

Table B.1: Coefficients of the X-variables for the respective Y-variable for the fifth statistical analysis.

Variable	Dv50	Dv90	Span	APD	SSA
Constant	13.05	7.93	13.27	7.28	3.74
Grinding pressure	-0.87	-0.94	-0.90	-0.81	0.84
Feed rate	0.29	0.31	0.30	0.27	-0.28

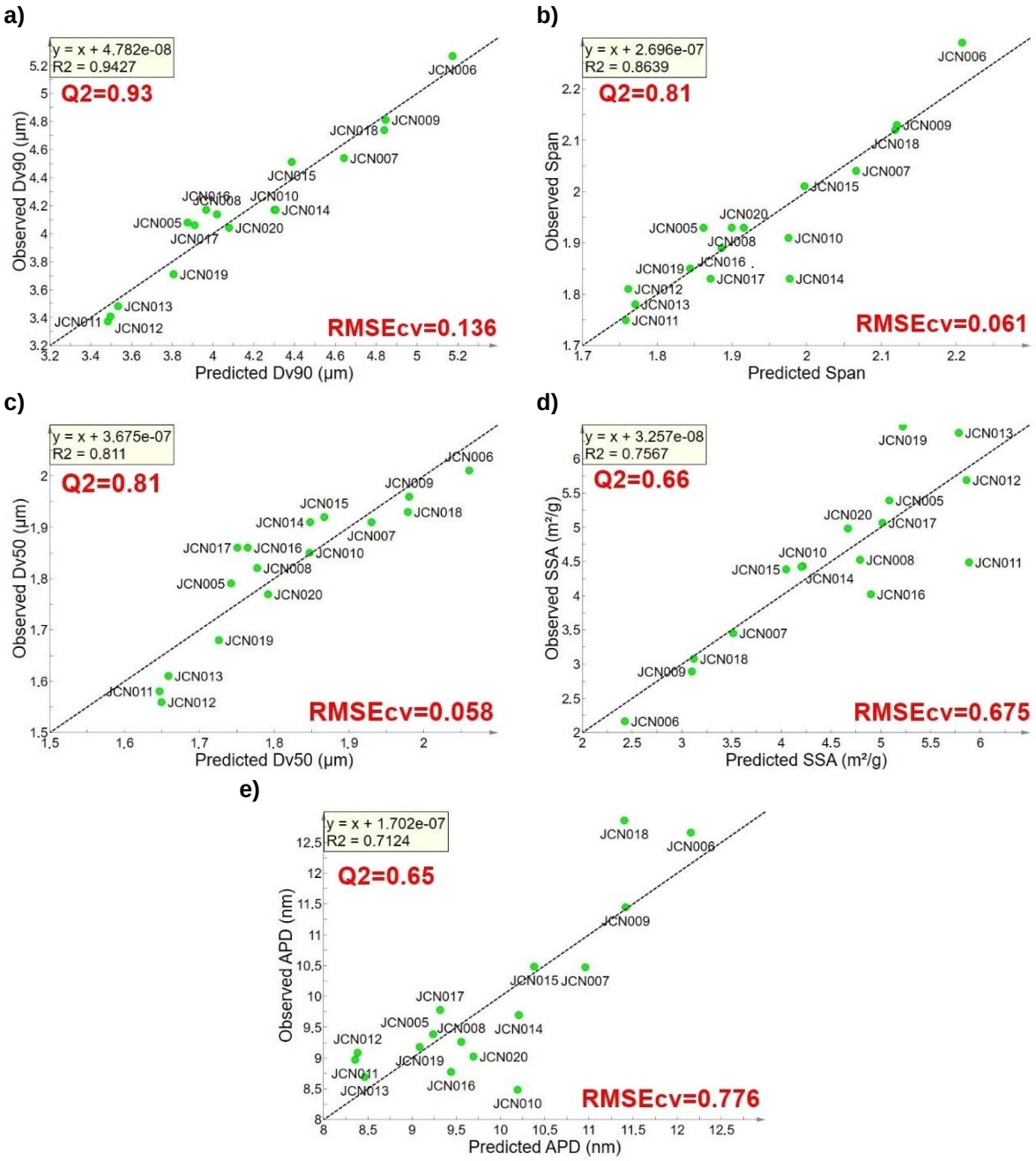

Figure B.5: Observed vs Predicted plots for a) Dv90, b) span, c) Dv50, d) SSA and e) APD for the fifth statistical analysis.

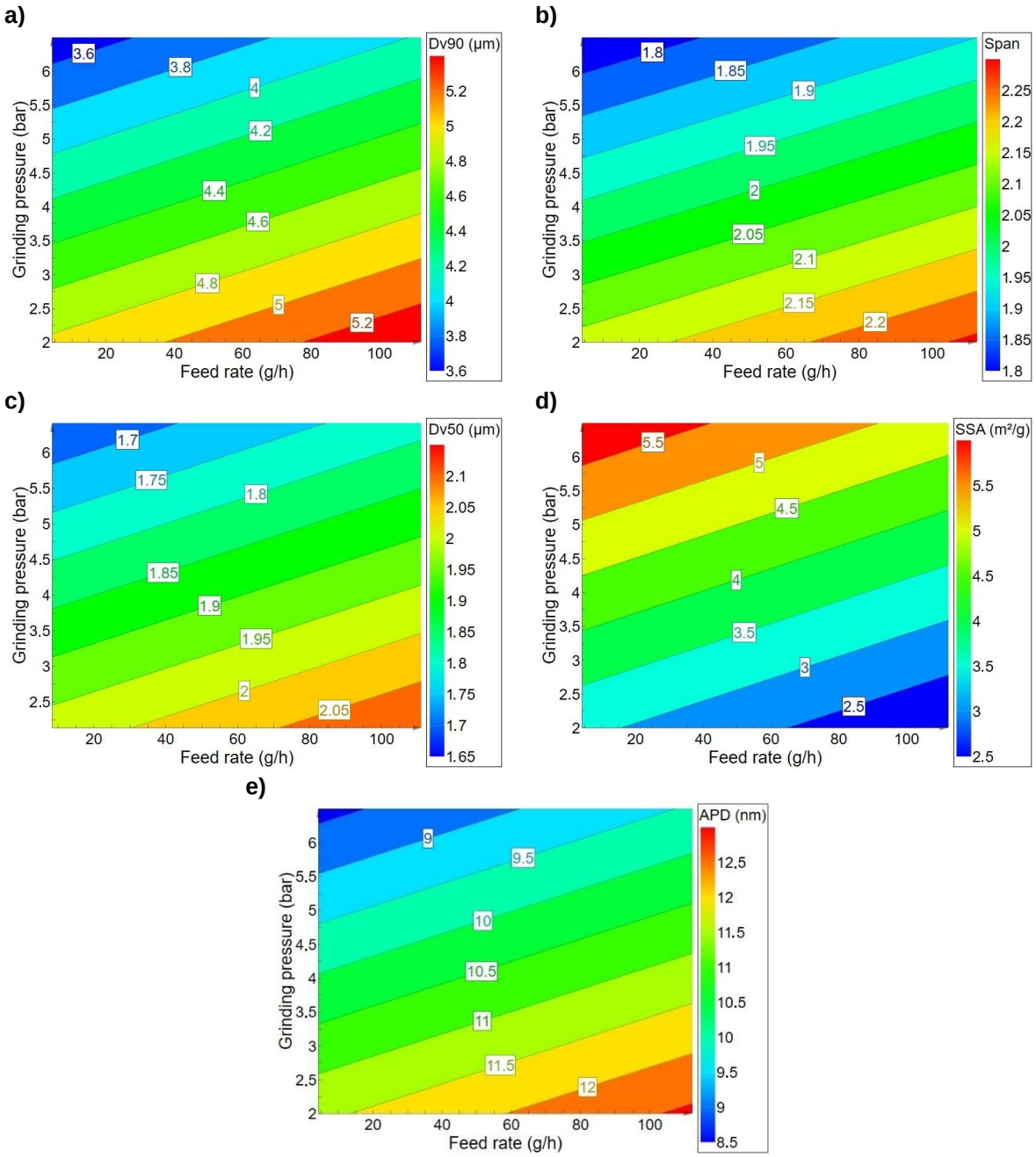

Figure B.6: Contour plots representing the variation of a) Dv90, b) span, c) Dv50, d) SSA and e) APD as a function of grinding pressure and feed rate for the fifth statistical analysis.